SIMCor

In-Silico testing and validation of Cardiovascular IMplantable devices

Call: H2020-SC1-DTH-2018-2020 (Digital transformation in Health and Care)

Topic: SC1-DTH-06-2020 (Accelerating the uptake of computer simulations for testing medicines and medical devices)

Grant Agreement Number: 101017578

Deliverable 8.4

Validated constitutive models of the vessel wall

Due date of delivery: August 31, 2022

Actual submission date: February 28, 2023

Start of the project: 1 January 2021
End date: 31 December 2023

This project has received funding from the European Union's Horizon 2020 research and innovation programmeunder grant agreement N° 101017578

References

Name	SIMCor_D8.4_Validated-constitutive-models-of-the-vessel-wall_TUG_28-02-2023
Lead beneficiary	Graz University of Technology (TUG)
Author(s)	Malte Rolf-Pissarczyk (TUG), Michele Terzano (TUG)
Dissemination level	Public
Type	Report
Official delivery date	31/08/2022
Date of validation by the WP Leader	28/02/2023
Date of validation by the Coordinator	28/02/2023
Signature of the Coordinator	Jan Bruening Digitally signed by Jan Bruening Date: 2023.02.28 15:06:03 +01'00'

Version log

Issue date	Version	Involved	Comments
03/08/2022	1.1	Malte Rolf-Pissarczyk (TUG), Michele Terzano (TUG)	First draft by TUG
11/08/2022	1.2	Jan Brüning (CHA)	Project Coordinator's review
16/08/2022	1.3	Ingmar Stade (BIO), Valentina Lavezzo (PHI)	Internal review by BIO and PHI
22/08/2022	1.4	Anna Rizzo (LYN), Jan Brüning (CHA)	Final review and formal checking by LYN and CHA
31/08/2022	Final	Jan Brüning (CHA)	Submission by PC
20/02/2023	2.1	Malte Rolf-Pissarczyk (TUG), Michele Terzano (TUG)	First draft by TUG
24/02/2023	2.2	Anna Rizzo (LYN)	Project Coordinator's review
24/02/2023	2.3	Ingmar Stade (BIO), Valentina Lavezzo (PHI)	Internal review by BIO and PHI
28/02/2023	2.4	Anna Rizzo (LYN), Jan Brüning (CHA)	Final review and formal checking by LYN and CHA
28/02/2023	Final	Jan Brüning (CHA)	Submission by PC

Executive summary

The deliverable reports the mechanical experiments and multi-photon microscopy imaging methods used to obtain the mechanical parameters and microstructural information of the ascending aorta and the pulmonary artery (main, left and right pulmonary artery) from healthy sheep, porcine and human tissue. In particular, the test set-up, the test protocol and the test samples are described for the biaxial extension test and the test protocol of the multi-photon microscopy method is detailed. Subsequently, the test results are presented. Lastly, based on the simplified vessel model (*Deliverable 8.3 - Constitutive vessel model (TUG, M20)*), an optimisation method is described to identify the constitutive parameters based on experimental data obtained from the literature and our laboratory.

Table of contents

List of figures

List of tables

Acronyms

Acronym	Full name
TAVI	Transcatheter Aortic Valve Implantation
PAPS	Pulmonary Artery Pressure Sensor
SHG	Second Harmonic Generation
MPM	Multi-Photon Microscopy
TPE	Two-Photon Excited
NDD	Non-Descanned Detector
PBS	Phosphate Buffered Saline
TUG	Graz University of Technology
BABB	Benzyl Benzoate
LYN	Lynceus
CHA	Charite
BIO	Biotronic

Introduction

The objective of SIMCor is to offer a comprehensive in-silico platform for manufacturers of cardiovascular implants to test and validate new devices. The platform specifically addresses the simulation of device effects on two representative areas: *transcatheter aortic valve implantation* (TAVI) and *pulmonary artery pressure sensors* (PAPS). Accurately simulating the implantation of a device requires the modelling of its physical properties, which include material, structural, geometric, and mechanical features of its components. In addition, the interaction with the tissue requires an accurate characterisation of mechanical properties and microstructure of the vessel wall, together with the development and validation of an appropriate constitutive model.

The scope of this document is to report all the relevant information regarding the two test methods, biaxial extension tests and *multi-photon microscopy* (MPM) imaging, and the related parameter identification. For this purpose, the tests methods are described briefly in *Section Test methods*; the test results are then reported in *Section Test results*. Finally, details of the parameter identification are provided in *Section Parameter identification*.

Test methods

This section will first provide a description of the process for harvesting and preparing the samples, before delving into the details of the two test methods - biaxial extension tests and MPM combined with *second-harmonic generation* (SHG) imaging. Please note that the sample harvesting process described is specific to porcine tissue (Marcher, Fleischwerke, Graz, Austria), as we received the sheep (Biotronik SE & Co. KG, Berlin, Germany) and human samples (Universitätsmedizin Rostock, Rostock, Germany) already prepared.

Sample harvesting

The heart, still connected to the lungs, of a freshly slaughtered pig as can be seen in *Figure* 1 (a) was collected in the morning from a nearby butcher. The preparation began with the removal of the pericardium as shown in *Figure* 1 (b). Usually, a lot of connective tissue surrounded the pulmonary artery and the ascending aorta. The tissue had to be cautiously removed to avoid damaging the blood vessels mentioned earlier. The ascending aorta and main pulmonary artery could then be separated as depicted in *Figure* 2 (a). Next, the left pulmonary artery was cut free from the lung and marked so that it will not be confused with the right pulmonary artery later. The same was done with the right pulmonary artery shown in *Figure* 2 (b), leaving only the ascending aorta and pulmonary artery connected to the heart as can be seen *Figure* 2 (c). At the end ascending aorta and main pulmonary artery were separated from the heart. The samples were put in tubes containing ringer lactate solution + 10% Dimethyl sulfoxide, also known as DSMO, and frozen at -80 °C.

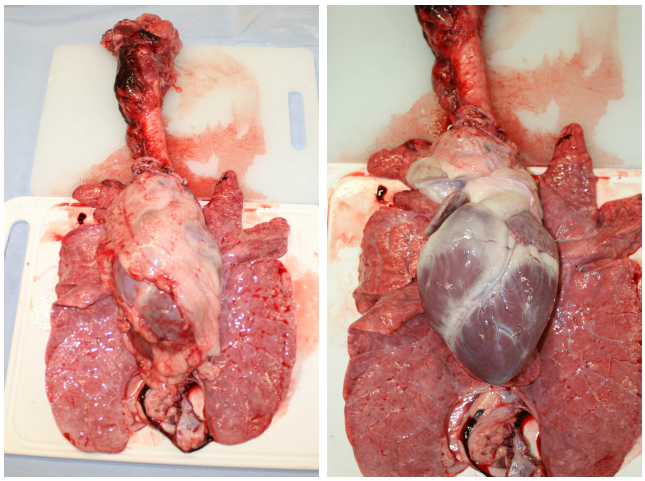

(a) *(b)*

Figure 1: Heart-lung complex from a freshly slaughtered pig with (a) and without pericardium (b).

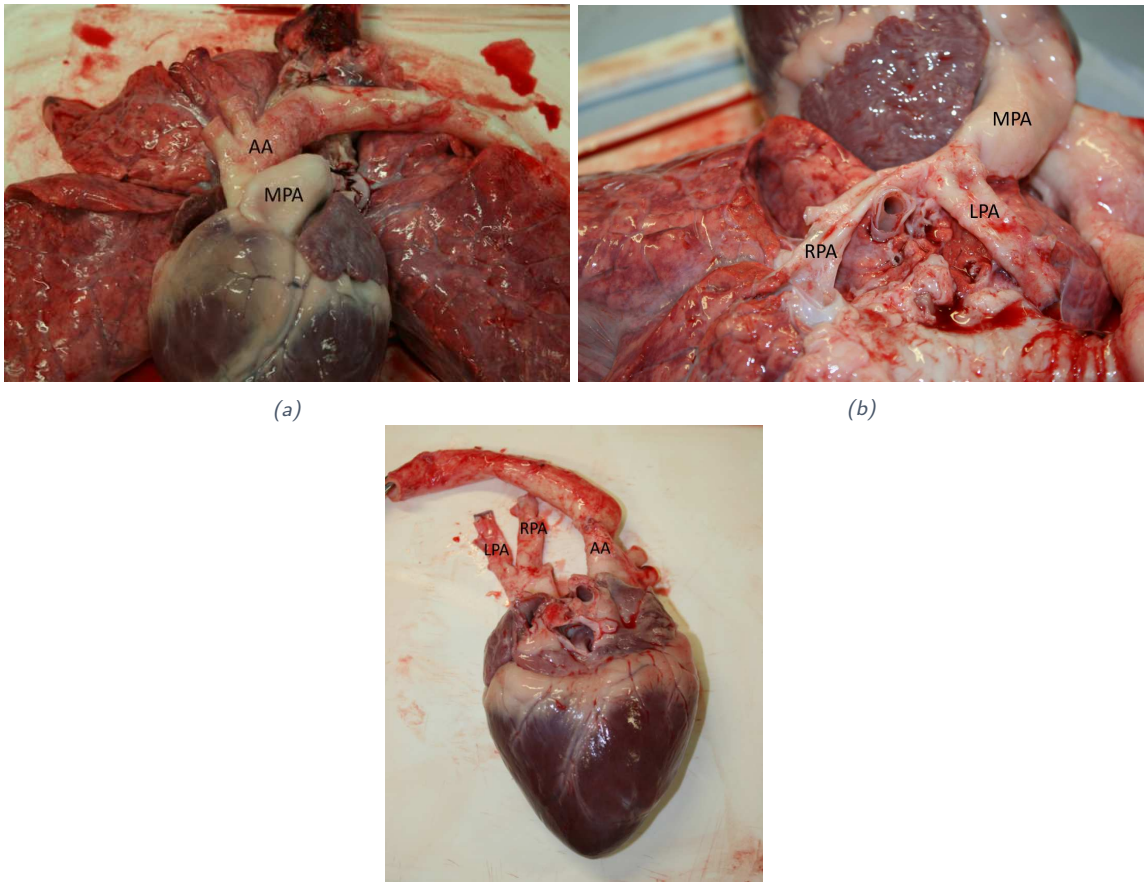

(a) *(b)*

(c)

Figure 2: Ascending aorta and main pulmonary artery without connective tissue (a). In (b) the left pulmonary artery is cut free and right pulmonary artery still connected to the lung. Picture (c) shows the backview of the heart with the pulmonary artery and ascending aorta.

Sample preparation

Loose connective tissue was removed from the defrosted samples, before cut open along the axial direction. Square samples measuring 10×10 mm were acquired from the anterior side of the proximal end as shown in the two examples of a right pulmonary artery and ascending aorta in *Figures* 3 and 4. The axial side was labeled to avoid any potential confusion with the circumferential direction. Adjacent to the square specimen a rectangular patch of dimension 5×10 mm was cut for histological examination (*Figure* 5). For orientation aid at the microscope, one edge was cut off. This specimen for imaging was stored in a tube filled with formaldehyde 4 %.

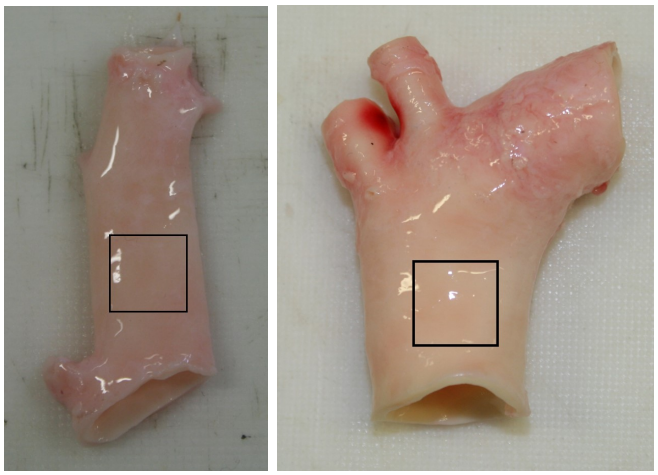

(a) (b)

Figure 3: Right pulmonary artery (a) and ascending aorta (b) before cutting open with highlighted spot from where the sample is taken from.

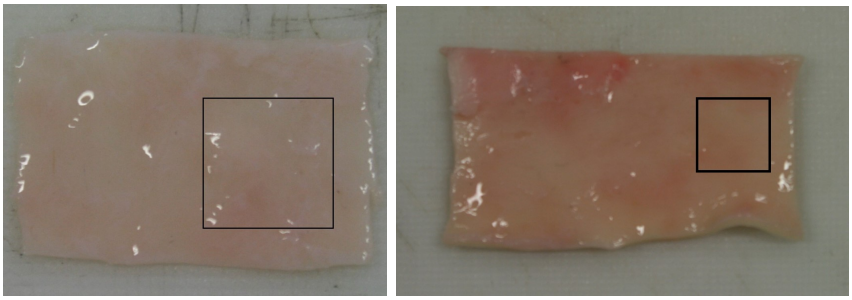

(a) (b)

Figure 4: Right pulmonary artery (a) and ascending aorta (b) after cutting open with highlighted spot from where the sample is taken from.

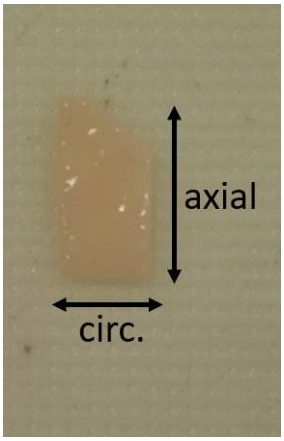

Figure 5: Sample from the right pulmonary artery for SHG imaging before optical clearing.

Biaxial extension tests

Test set-up

The setup of the biaxial extension test used in the laboratory of the Institute of Biomechanics at *Graz University of Technology* (TUG) is illustrated in *Figure* 6. The planar biaxial extension testing device employed integrates four linear actuators, which can be controlled independently by position, force or stretch. The force measurement is conducted by submersible load cells: two in the circumferential direction and two in the axial direction, which are connected to a clamping device. The maximum testing load is specified at 100 N per sensor and a resolution of 0.6 mN is achieved. The maximum travel range is 50 mm (with a resolution of 0.1 μm) for each linear actuator, and the maximum speed is limited to approximately 30 mm/s. Another feature of this biaxial extension testing device is the videoextensometre, which allows two-dimensional, non-contact stretch measurements by tracking markers which are fixed onto the surface of the specimen. A resolution of 0.15 μm of the videoextensometre is specified by the manufacturer.

Protocol

Every sample was mounted with 3 hooks at each side, which were placed homogeneously on a square of approximately 10×10 mm, as shown in *Figure* 6(a). Due to the roller, the forces were applied (nearly) uniformly to the 3 hooks. Also, the samples were randomly dotted with black markers for the displacement tracking. Once mounted on the system, the samples were preloaded and then the displacement was set to zero before starting the full test. Finally, the tank was filled with *phosphate buffered saline* (PBS) heated at 37 °C.

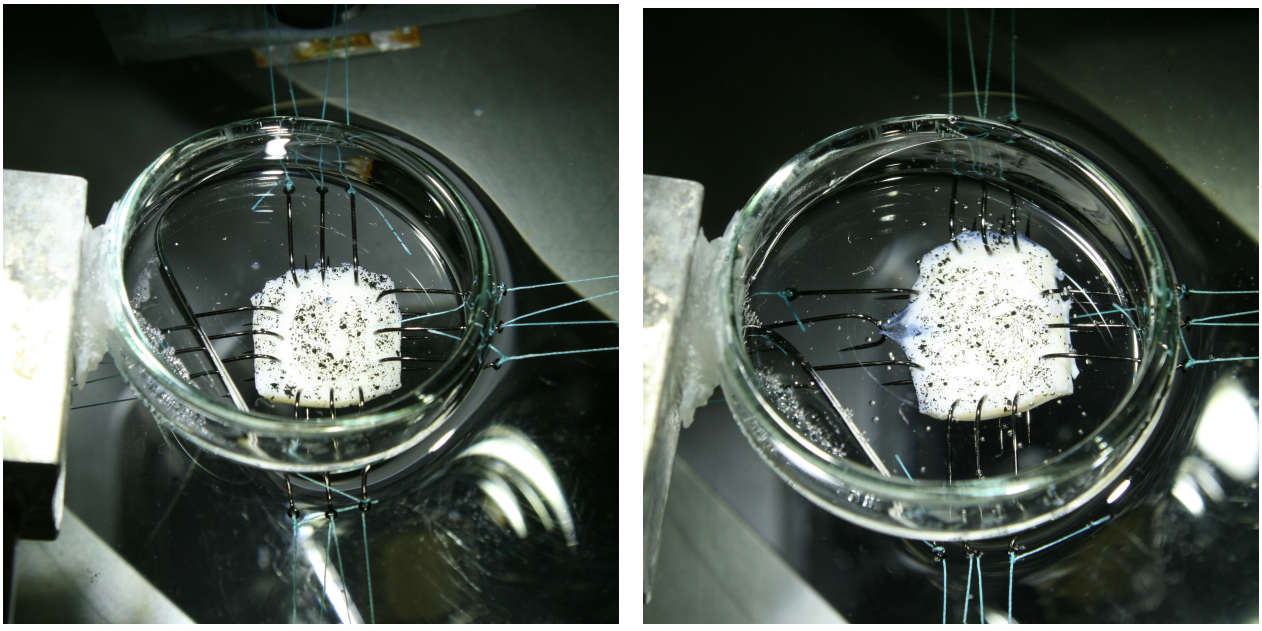

(a) *(b)*

Figure 6: Exemplary tissue sample mounted in the biaxial extension testing device with an applied load (a) and the failure of the hooks at large stretches (b).

To control the biaxial extension test, in-plane deformations of the samples are recorded by means of a CCD camera. The tracking software 'Laser Speckle Extensometer' evaluates the displacement of the markers fixed onto the sample surface in real time.
The following test parameters were used:

- Preload: $<$0.015 N
- Strain rate (engineering): 3 mm/min
- Stretch levels: 1.1, 1.2, ... (until failure)
- Preconditioning: 5 cycles
- Strain ratios: 1:1, 1:0.75, 0.75:1, 1:0.5, 0.5:1 (circumferential/axial)
  (all strain ratios per each stretch level are completed before moving on to next stretch level)

Failure of the sample usually occurs due to the pull-out of the hooks at large stretches, as shown in *Figure* 6(b) for a representative sample.

Testing sampling

The following tissue samples were tested:

- Sheep tissue: 9
- Porcine tissue: 11
- Human tissue: 5

The biaxial extension test results for the tissue samples are made available to the consortium members as supplementary material (VRE Drive). For each sample, the data is given in the form of .xls files. The .xls files include the biaxial extension tests of samples of all stretch levels. For each stretch level, we applied 5 preconditioning cycles which were followed by five strain ratios (1:1, 1:0.75, 0.75:1, 1:0.5, and 0.5:1), as described previously. The data in the .xls-files are structured as follows:

1. Time (s)
2. Displacement 1 (mm)
3. Force 1 (N)
4. Displacement 2 (mm)
5. Force 2 (N)
6. Displacement 3 (mm)
7. Force 3 (N)
8. Displacement 4 (mm)
9. Force 4 (N)
10. Stretch 1-2 (–)
11. Stretch 3-4 (–)
12. Initial distance 1-2 (mm)
13. Initial distance 3-4 (mm)
14. No. of cycles (–)

To obtain the force in the circumenferential and axial direction, respectively, we computed the mean force for the two directions (circumferential: 1-2, axial: 3-4). We were unable to do this in certain cases due to partial malfunctioning in load cells 4 and 1. The equations for calculating then the different mechanical quantities are given below:

- Engineering strain:
  $\epsilon_e = \frac{l-L_0}{L_0}$, where l in (mm) is the current extension and L_0 in (mm) is the initial length between the two markers.
- Engineering stress:
  $P = \frac{F}{TL}$, where T is the sample thickness, F is the current load, and L is the sample width.
- Cauchy stress:
  $\sigma = P(1 + \epsilon_e)$

Multi-photon microscopy (MPM)

The following section provides a detailed imaging protocol for MPM, which is utilised to examine sheep, porcine, and human tissue samples. The imaging procedure entails performing SHG imaging in both in-plane and out-of-plane directions. It is worth noting that, in the context of the vessel wall, "in-plane" and "out-of-plane" refer to the orientation of structural features, specifically collagen fibres, within the wall. Collagen fibres serve as a vital structural component of the extracellular matrix of the vessel wall, supplying tensile strength and resisting deformation. The in-plane distribution of collagen fibres pertains to their orientation parallel to the surface within the plane of the wall (circumferential-axial plane). Conversely, the out-of-plane distribution refers to their orientation perpendicular to the plane of the wall (axial-radial plane).

Imaging protocol

The imaging procedure was carried out at the Institute of Molecular Biosciences (Graz, Austria) Optical Imaging Resource with a tunable picosecond laser (picoEmerald; APE, Berlin, Germany), which is integrated into a Leica SP5 confocal microscope (Leica Microsystems, Mannheim, Germany). The laser is tuned to 880 nm to induce both the SHG signal from collagen and the *two-photon excited* (TPE) autofluorescence signal from elastin, although the signal from collagen is of primal interested for this delivery. A two-channel, *non-descanned detector* (NDD) in epi-mode is used to detect SHG and TPE signals simultaneously (SP 680 nm barrier filter, i.e., excitation light filter; BP 460/50 nm for SHG signal; BP 525/50 nm for TPE signal; beamsplitter RSP 495 for two-channel separation of SHG and TPE signals). So-called Z-stacks are acquired with the HCX IRAPO L 25x NA 0.95 water immersion objective with a large working distance of 1.5 mm for imaging the deep tissue and a sampling interval of $0.6 \times 0.6 \times 5.0\,\mu$m. As a compromise between image quality and acquisition time, a line average of 8 four-fold line averaging is used to reduce image noise. A coverglass and water as the immersion medium can not be used with samples mounted on the biaxial test device, since the coverglass cannot be fixed horizontally and the sample quickly soaked up water. Alternatively, an aqueous eye gel Lac-Ophtal Gel (Dr. Winzer Pharma, Berlin, Germany) is used, and the lens is dipped directly into the gel. This protocol was recently described by Pukaluk et al. [3].

Optical clearing

The samples were cleared using the protocol according to Schriefl et al. [4]. First the samples were rinsed twice in PBS, followed by a graded ethanol series for dehydration. Each step lasted 45 min starting with 50 %, 70 %, followed twice each by 95 % and 100 % concentrated ethanol solution. The optical clearing itself was conducted with a 1:2 benzyl alcohol to *benzyl benzoate* (BABB) solution. The samples were cleared with a 1:1 solution of ethanol:BABB for 4h. Subsequent to that, the subjects were immersed in a 100 % BABB solution for a minimum of 12 hours prior to imaging. All steps described were performed at room temperature.

Testing samples

The following tissue samples were analysed:

- Sheep: 4
- Porcine: 2

In late January, the MPM located at the Institute of Molecular Biosciences (Graz, Austria) failed due to technical damage sustained by the laser and its cooling system. Due to high costs of repairing this device, there was no immediate solution available, and as a result, we were unable to image any more samples for this deliverable. However, we have now secured an alternative at the Core Facility Bioimaging (Munich, Germany). They confirmed that their modern MPMs have available capacities over the next months. As soon as we completed imaging the remaining samples, we will share the results with our project partners internally.

Test results

Biaxial extension tests

Below are the findings from the biaxial extension tests conducted on samples of sheep, porcine tissue, and human subjects. The figures show the Cauchy stress versus stretch during loading, for a strain ratio of 1:1 (equibiaxial) for each stretch level applied. Note that the tests were performed until failure of the hooks occurred, see *Figure* 6(b).

Sheep tissue

The results of the biaxial extension tests for sheep tissue are shown in *Figures* 7-10. In addition, the mean thickness and the sample size for each sample are listed in the Appendix (*Table* 6).

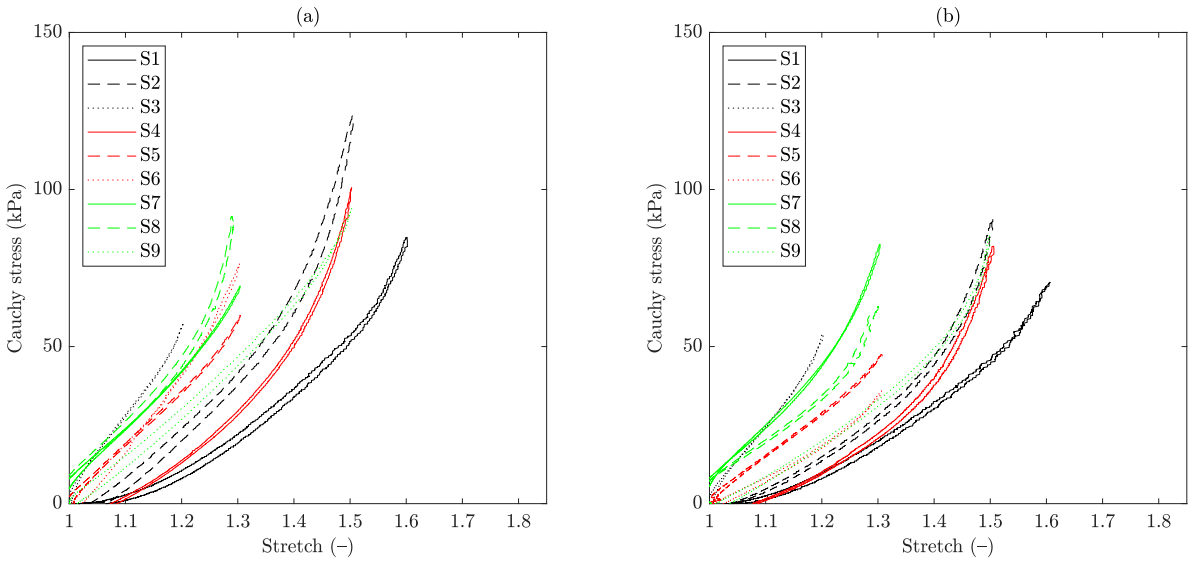

Figure 7: Biaxial extension test results of sheep ascending aorta (a) in circumferential and (b) axial directions (strain ratio of 1:1). The plots show the Cauchy stress versus stretch until failure of the sample.

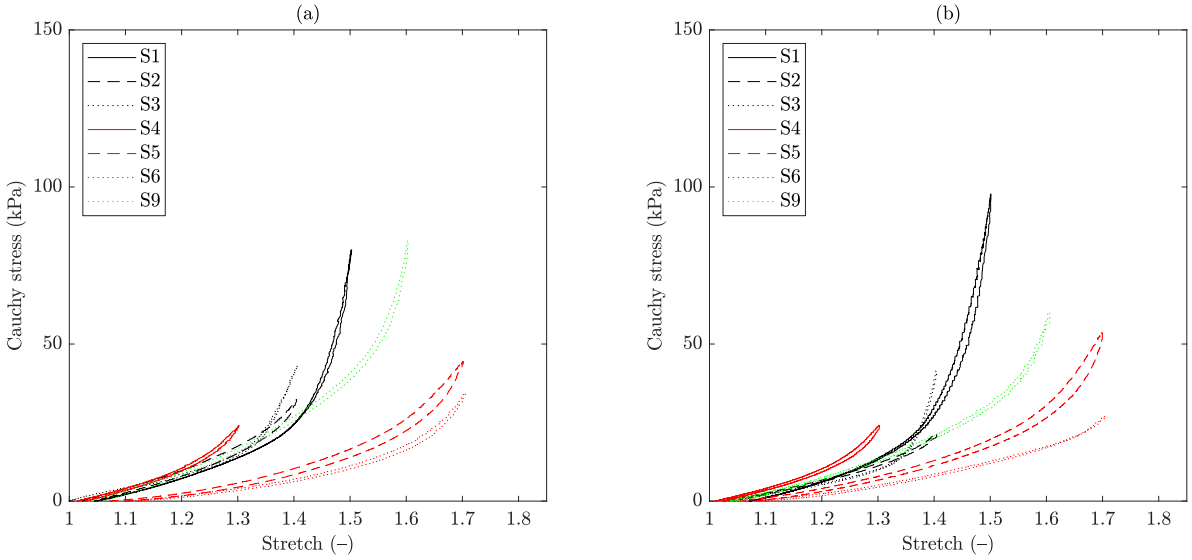

Figure 8: Biaxial extension test results of sheep main pulmonary artery (a) in circumferential and (b) axial directions (strain ratio of 1:1). The plots show the Cauchy stress versus stretch until failure of the sample.

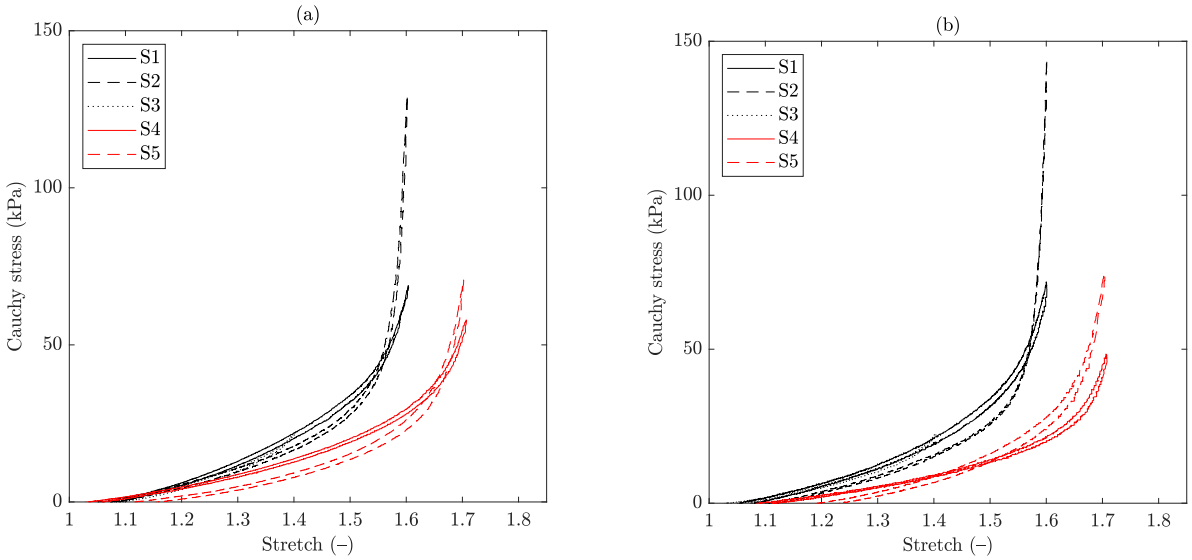

Figure 9: Biaxial extension test results of sheep left pulmonary artery (a) in circumferential and (b) axial directions (strain ratio of 1:1). The plots show the Cauchy stress versus stretch until failure of the sample.

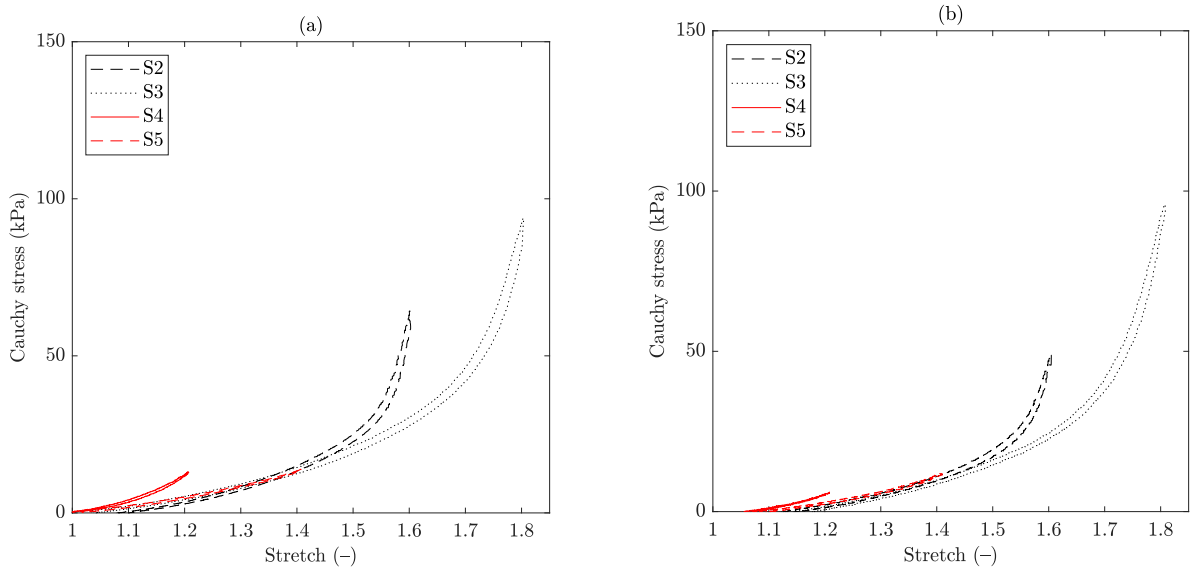

Figure 10: Biaxial extension test results of sheep right pulmonary artery (a) in circumferential and (b) axial directions (strain ratio of 1:1). The plots show the Cauchy stress versus stretch until failure of the sample.

Porcine tissue

The results of the biaxial extension tests for porcine tissue are shown in *Figures* 11-14. In addition, the mean thickness and the sample size for each sample are listed in the Appendix (*Table* 7).

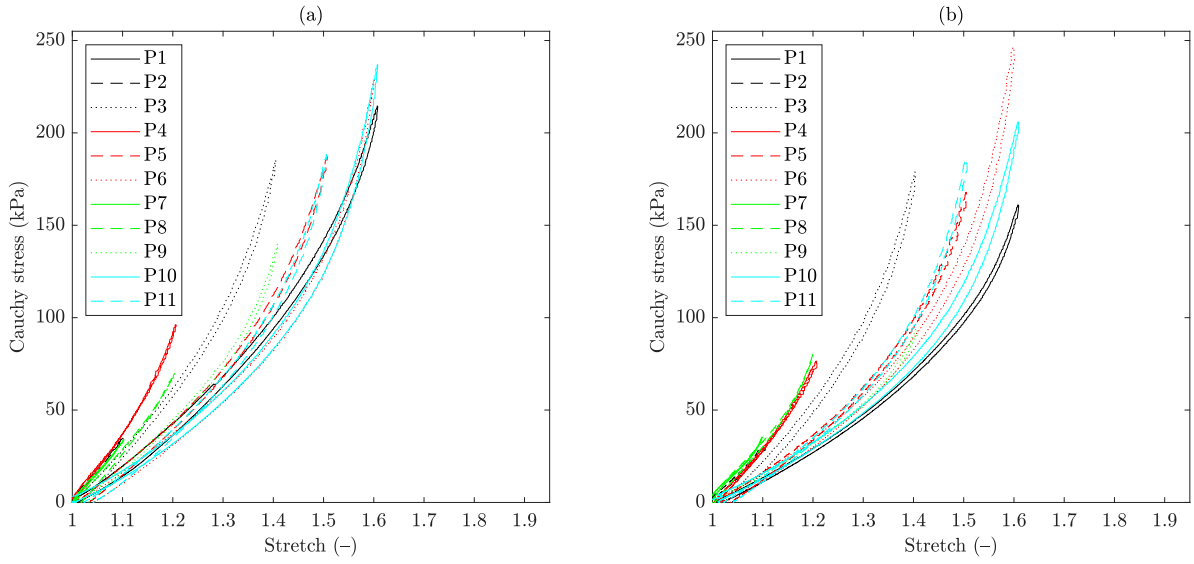

Figure 11: Biaxial extension test results of porcine ascending aorta (a) in circumferential and (b) axial directions (strain ratio of 1:1). The plots show the Cauchy stress versus stretch until failure of the sample.

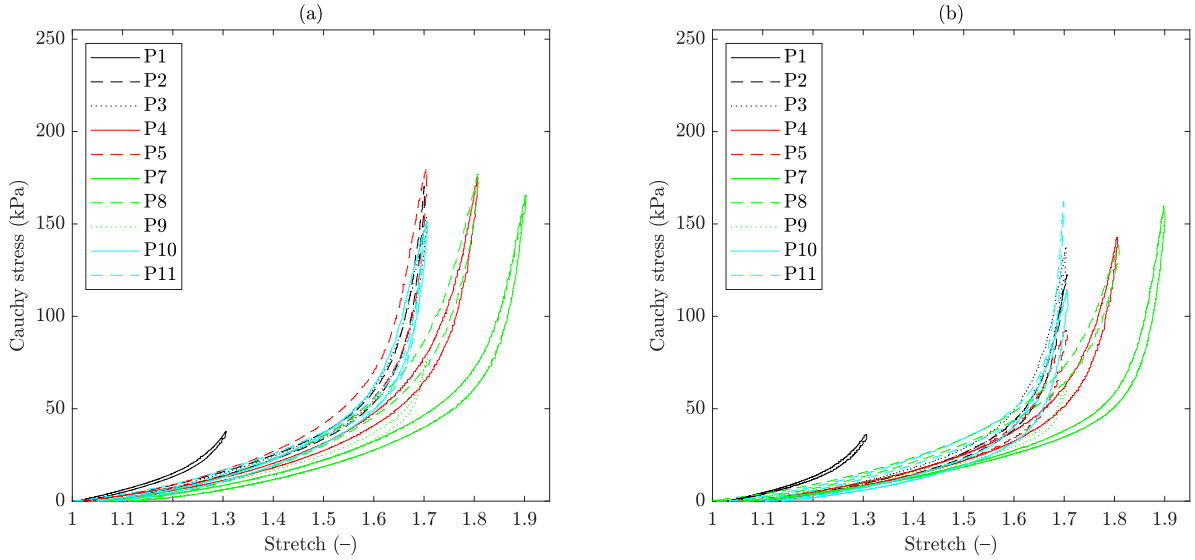

Figure 12: Biaxial extension test results of porcine main pulmonary artery (a) in circumferential and (b) axial directions (strain ratio of 1:1). The plots show the Cauchy stress versus stretch until failure of the sample.

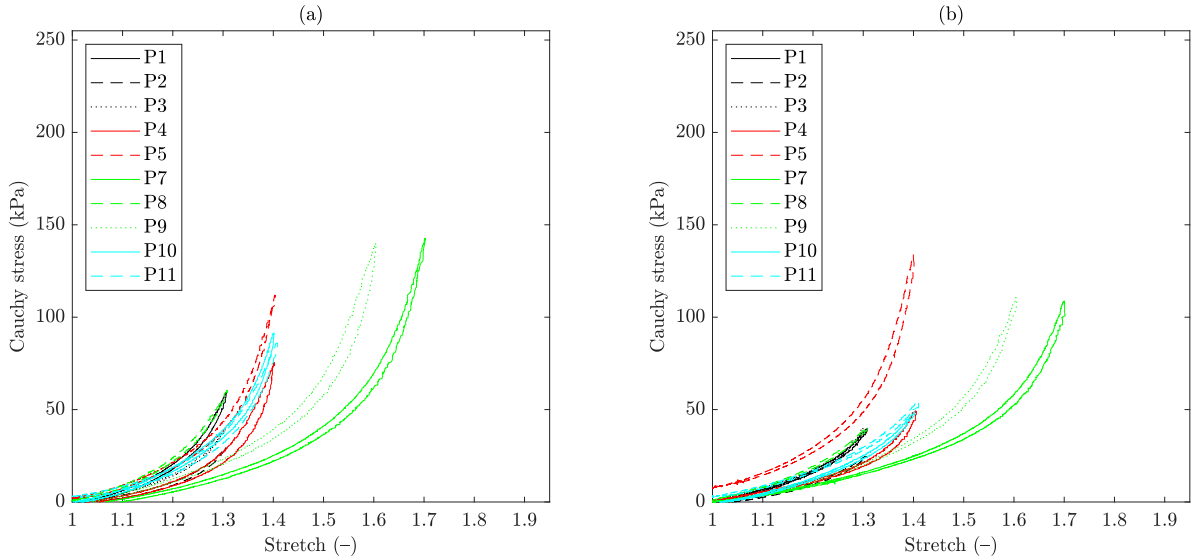

Figure 13: Biaxial extension test results of porcine left pulmonary artery (a) in circumferential and (b) axial directions (strain ratio of 1:1). The plots show the Cauchy stress versus stretch until failure of the sample.

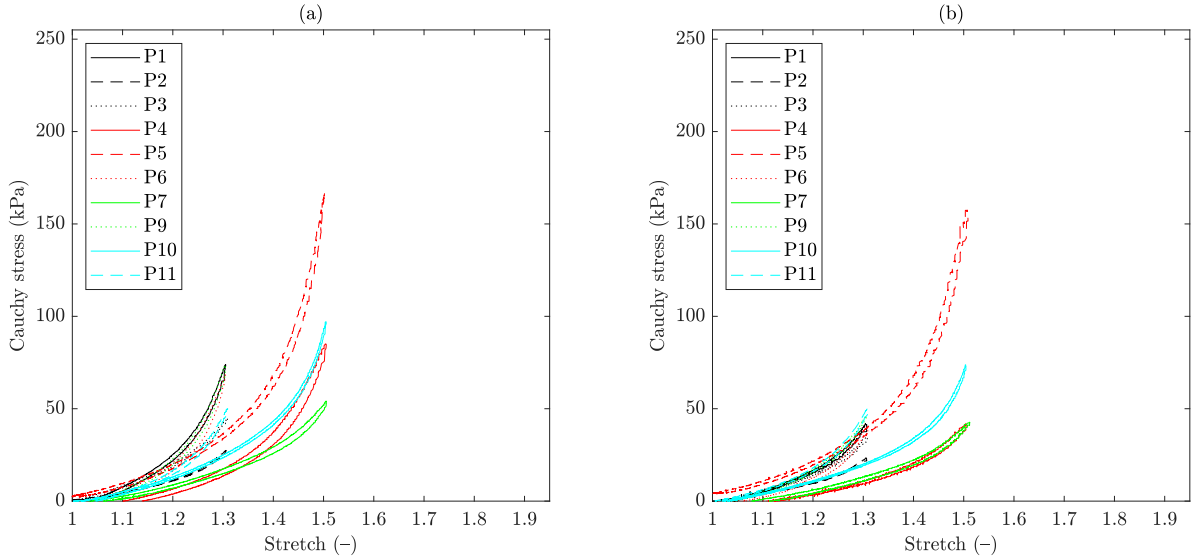

Figure 14: Biaxial extension test results of porcine right pulmonary artery (a) in circumferential and (b) axial directions (strain ratio of 1:1). The plots show the Cauchy stress versus stretch until failure of the sample.

Human tissue

The results of the biaxial extension tests for human tissue are shown in *Figures* 15-18. In addition, the mean thickness and the sample size for each sample are listed in the Appendix (*Table* 8).

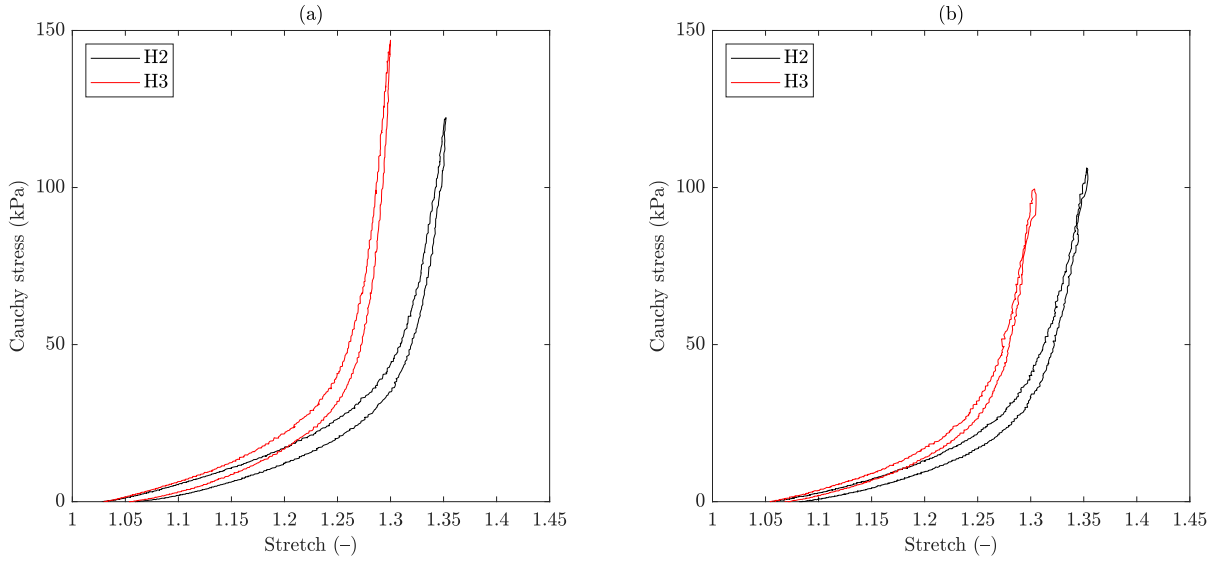

Figure 15: Biaxial extension test results of human ascending aorta (a) in circumferential and (b) axial directions (strain ratio of 1:1). The plots show the Cauchy stress versus stretch until failure of the sample.

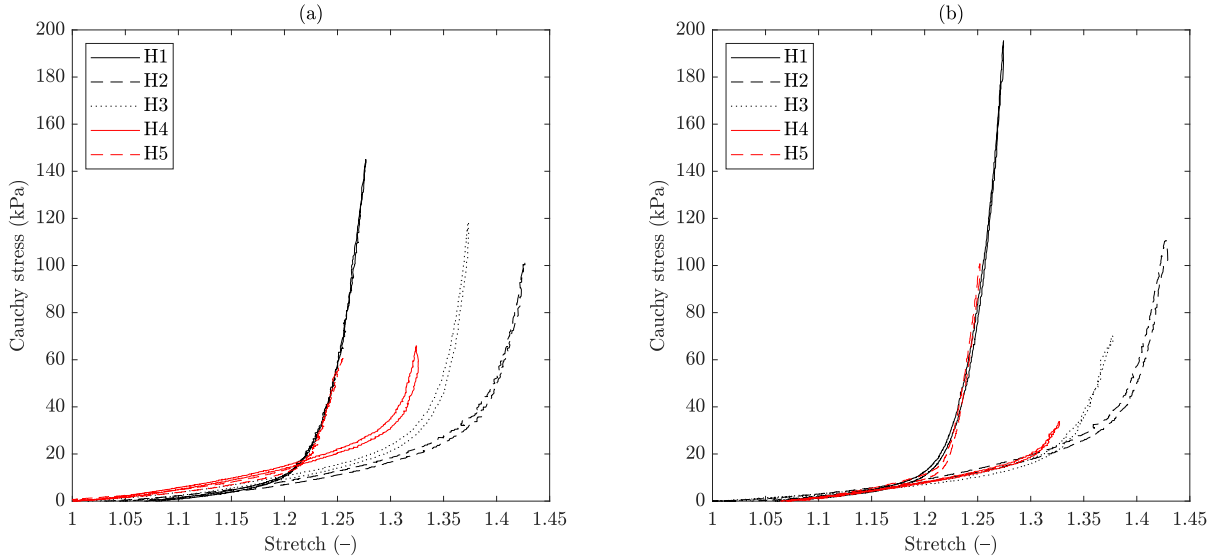

Figure 16: Biaxial extension test results of human main pulmonary artery (a) in circumferential and (b) axial directions (strain ratio of 1:1). The plots show the Cauchy stress versus stretch until failure of the sample.

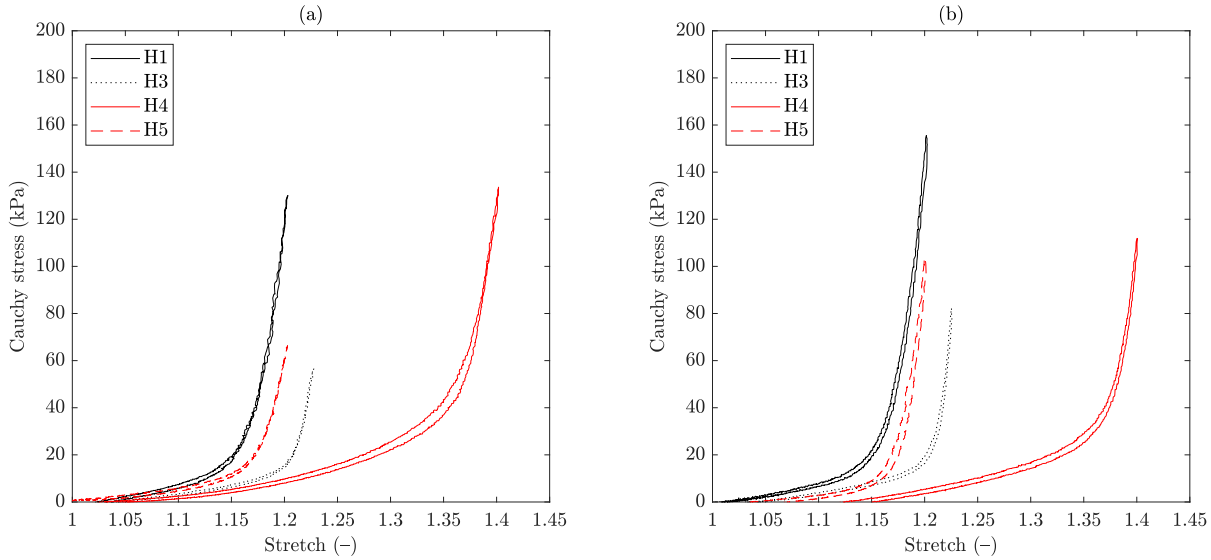

Figure 17: Biaxial extension test results of human left pulmonary artery (a) in circumferential and (b) axial directions (strain ratio of 1:1). The plots show the Cauchy stress versus stretch until failure of the sample.

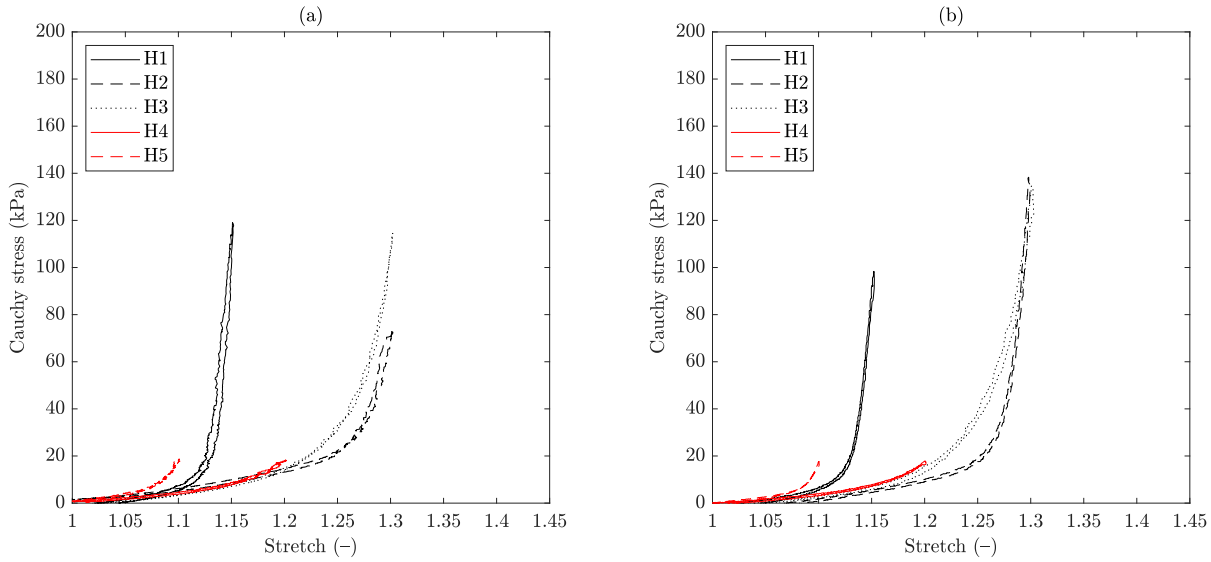

Figure 18: Biaxial extension test results of human right pulmonary artery (a) in circumferential and (b) axial directions (strain ratio of 1:1). The plots show the Cauchy stress versus stretch until failure of the sample.

Summary

In summary, the results show that the ascending aorta and the pulmonary artery behave differently. The ascending aorta usually has a high initial stiffness, which then increases slightly with increasing stretching, whereas the pulmonary artery has a low initial stiffness which then quickly increases at higher stretches. This could be related to the orientation, distribution and waviness of collagen fibres in the respective tissues. In general, sheep, porcine and human tissues behaved similarly with respect to the ascending aorta and pulmonary arteries. However, porcine tissue samples from the left and right pulmonary arteries failed significantly earlier than those from the main pulmonary artery. In addition, porcine and human samples tended to exhibit a slightly stiffer behaviour overall, with the human tissue showing a very peculiar low-stiffness initial region followed by a steep exponential increase of the stress during equibiaxial tests.

SHG imaging

The images below display the results of SHG imaging conducted on sheep and porcine tissue. The figures depict the probability density function of collagen fibres in both the in-plane and out-of-plane directions. As previously mentioned, "in-plane" refers to the direction that is parallel to the plane of the wall, while "out-of-plane" refers to the direction that is perpendicular to the plane of the wall. The in-plane distribution was obtained by averaging the probability density function across the full thickness of the vessel wall, while the out-of-plane distribution was obtained in the same manner for the chosen location.

Sheep tissue

The results of the SHG imaging for sheep tissue are shown in *Figures* 19-30.

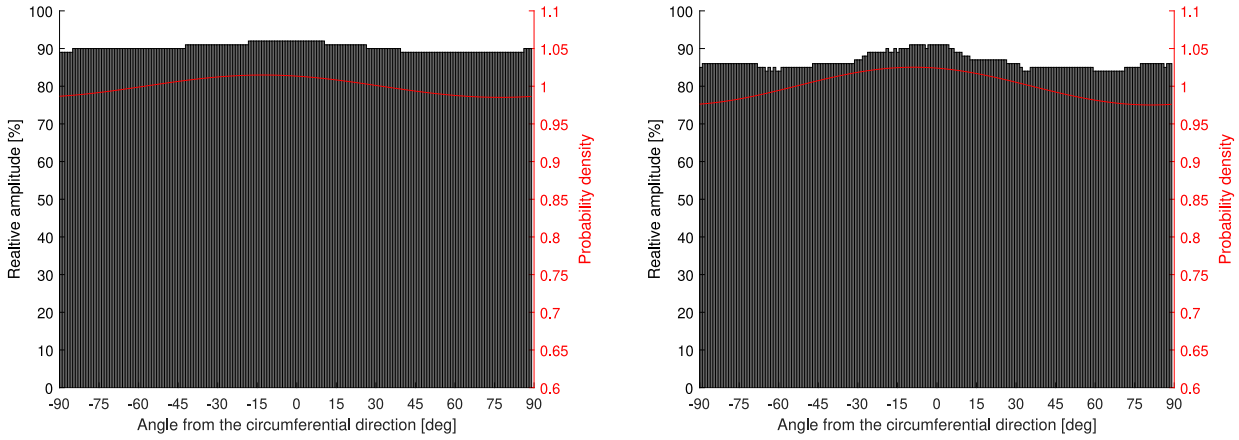

Figure 19: Probability density function of sheep (1) ascending aorta for collagen fibres in (a) in-plane and (b) out-of-plane directions.

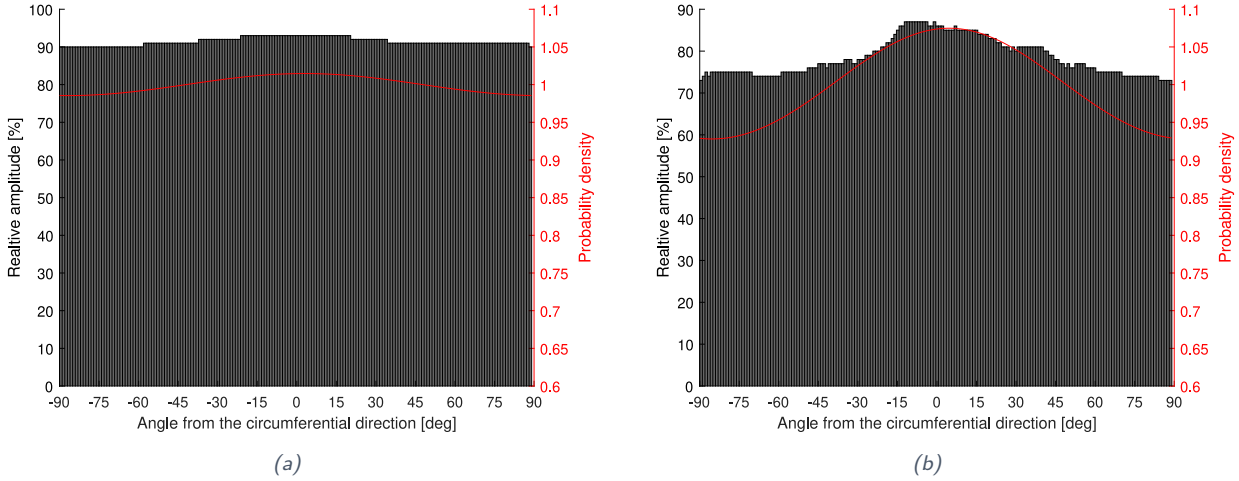

Figure 20: Probability density function of sheep (1) left pulmonary artery for collagen fibres in (a) in-plane and (b) out-of-plane directions.

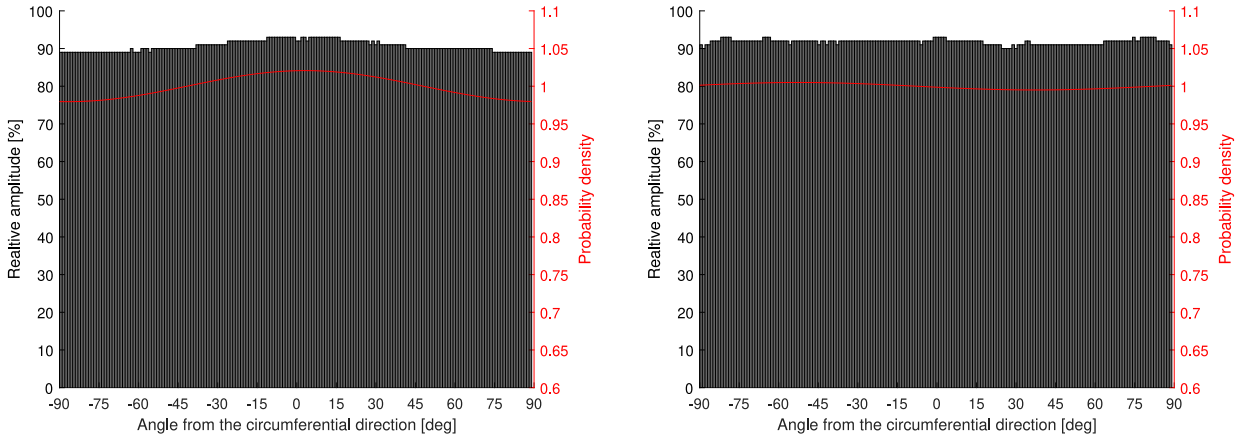

(a) *(b)*

Figure 21: Probability density function of sheep (1) main pulmonary artery for collagen fibres in (a) in-plane and (b) out-of-plane directions.

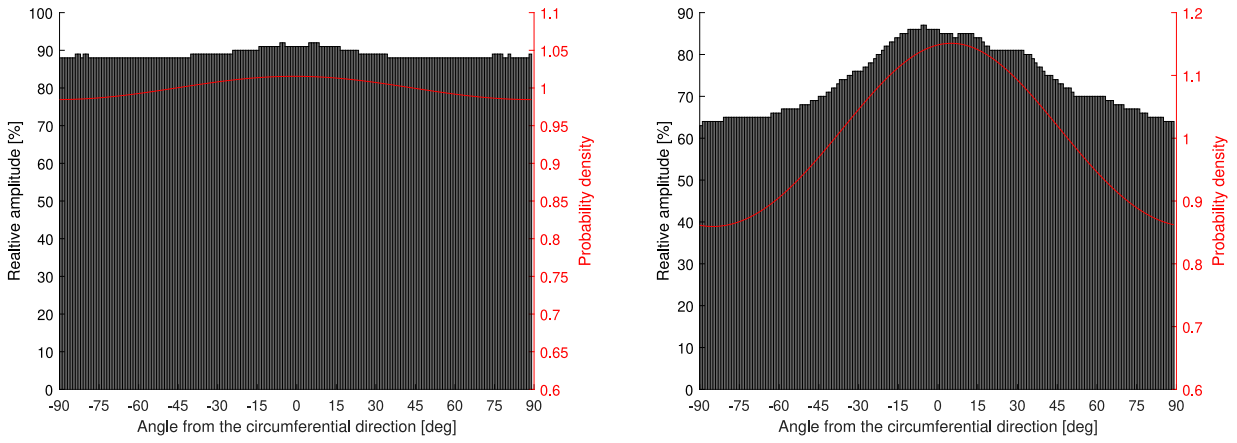

(a) *(b)*

Figure 22: Probability density function of sheep (2) ascending aorta for collagen fibres in (a) in-plane and (b) out-of-plane directions.

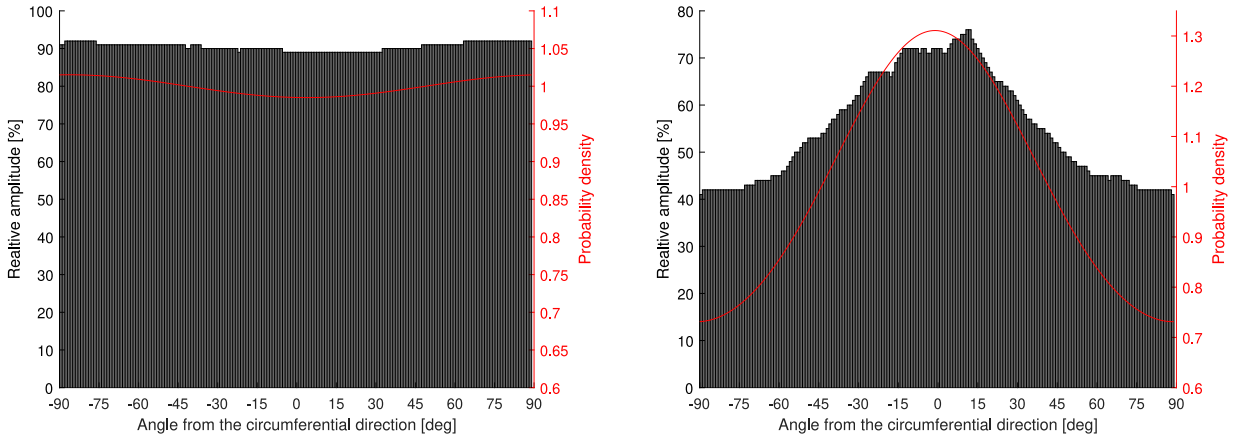

(a) *(b)*

Figure 23: Probability density function of sheep left pulmonary artery for collagen fibres in (a) in-plane and (b) out-of-plane directions.

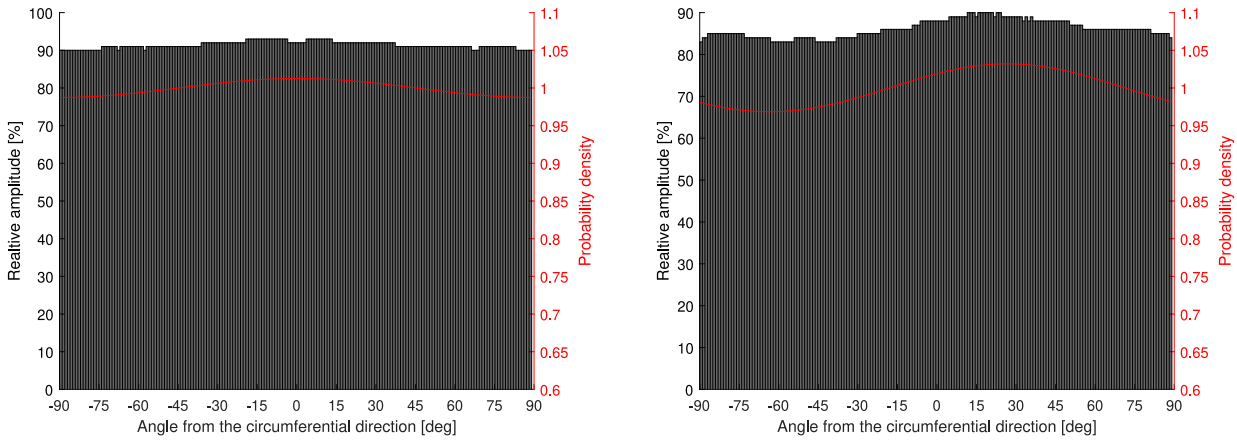

(a) *(b)*

Figure 24: Probability density function of sheep (2) main pulmonary artery for collagen fibres in (a) in-plane and (b) out-of-plane directions.

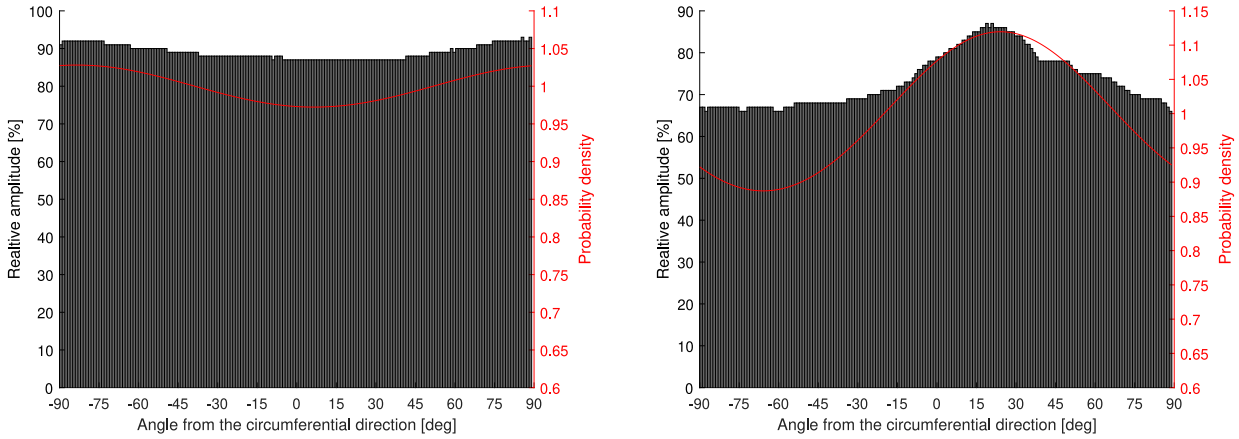

(a) *(b)*

Figure 25: Probability density function of sheep (2) right pulmonary artery for collagen fibres in (a) in-plane and (b) out-of-plane directions.

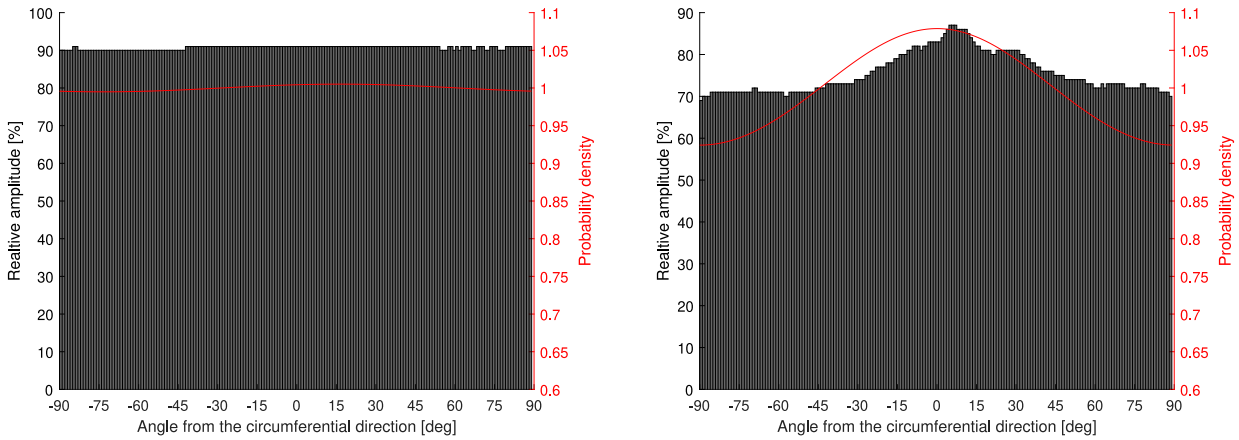

(a) *(b)*

Figure 26: Probability density function of sheep (3) ascending aorta for collagen fibres in (a) in-plane and (b) out-of-plane directions.

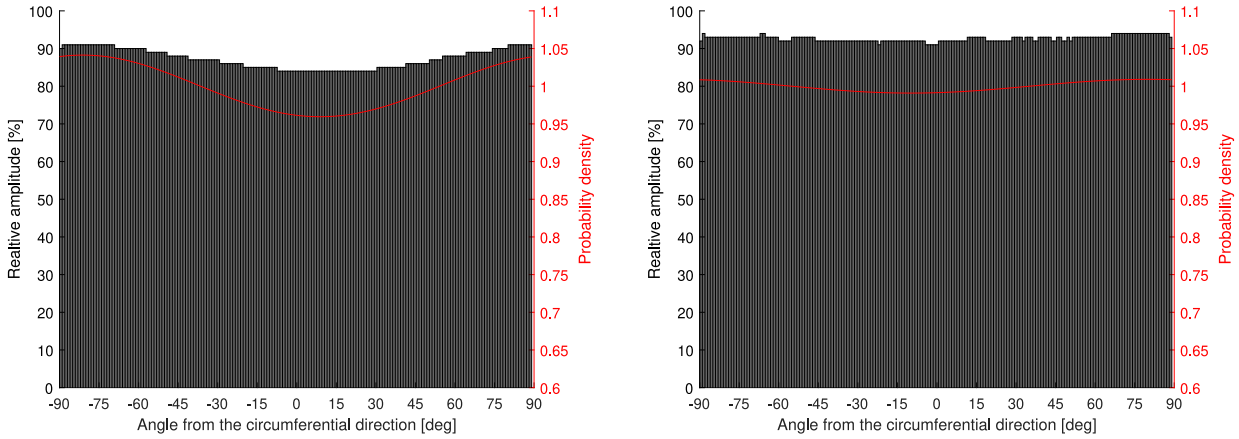

(a) *(b)*

Figure 27: Probability density function of sheep (3) left pulmonary artery for collagen fibres in (a) in-plane and (b) out-of-plane directions.

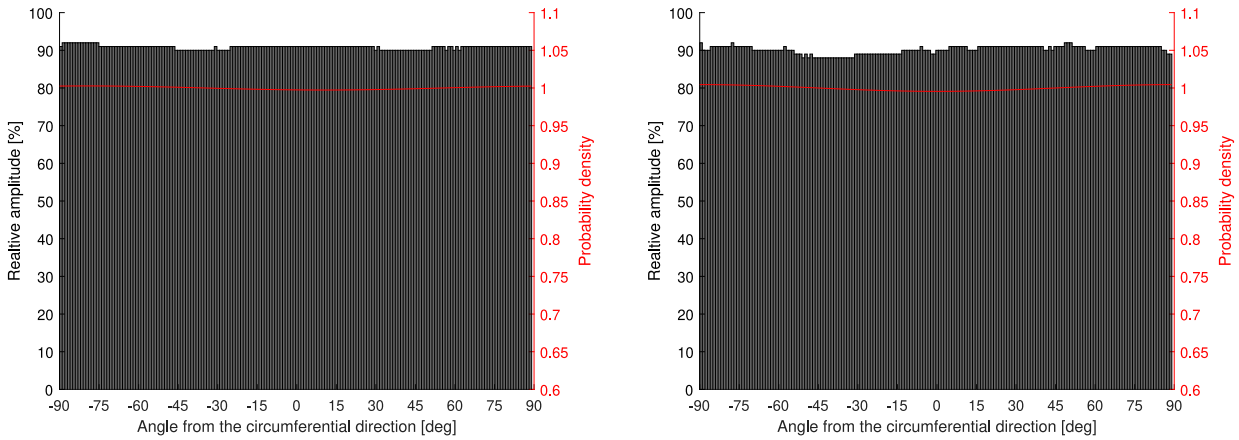

(a) *(b)*

Figure 28: Probability density function of sheep (3) right pulmonary artery for collagen fibres in (a) in-plane and (b) out-of-plane directions.

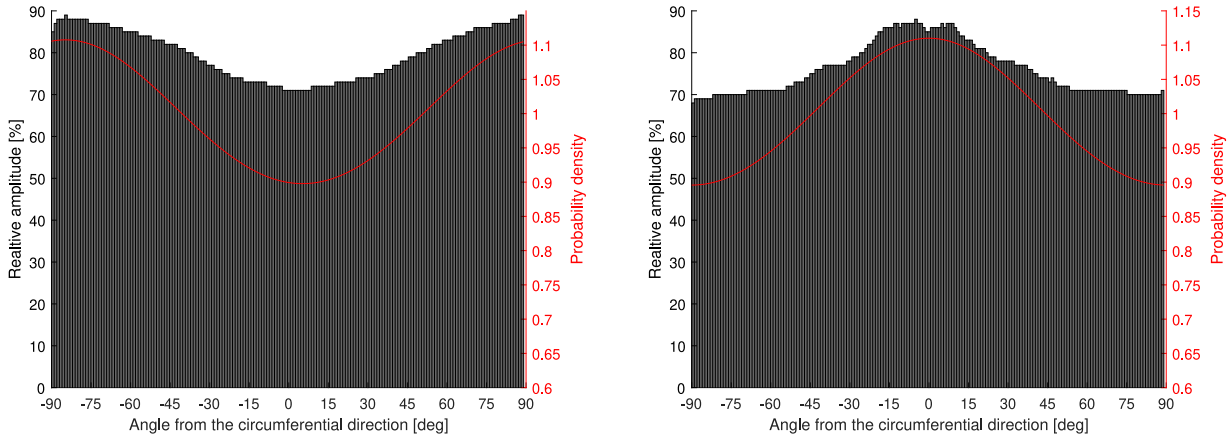

(a) *(b)*

Figure 29: Probability density function of sheep (4) left pulmonary artery for collagen fibres in (a) in-plane and (b) out-of-plane directions.

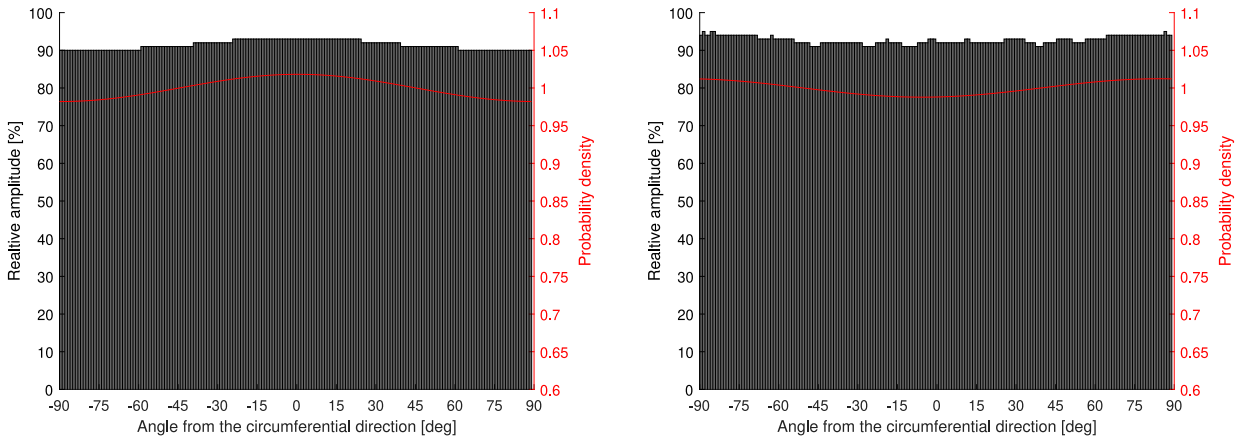

(a) *(b)*

Figure 30: Probability density function of sheep (4) main pulmonary artery for collagen fibres in (a) in-plane and (b) out-of-plane directions.

Porcine tissue

The results of the SHG imaging for porcine tissue are shown in *Figures* 31-37.

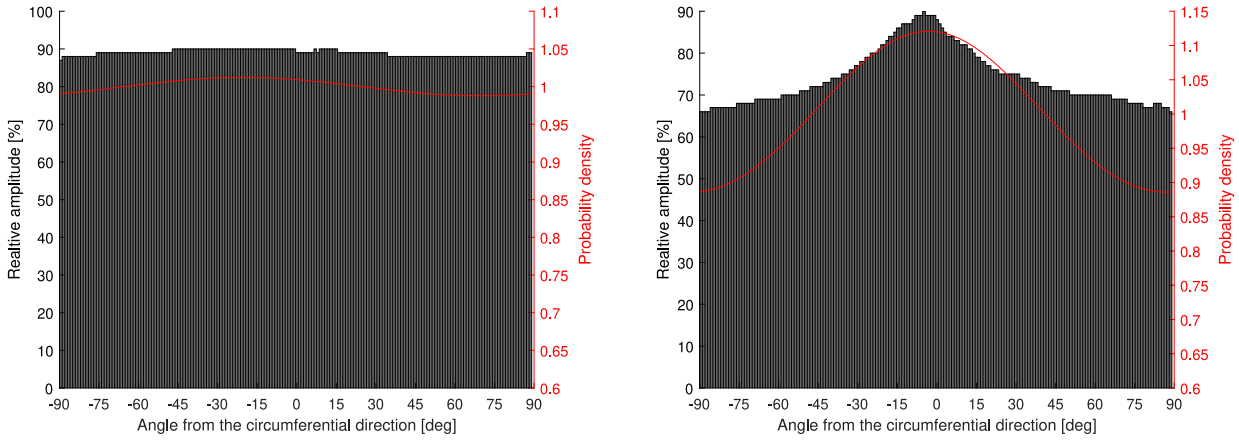

(a) *(b)*

Figure 31: Probability density function of porcine (1) ascending aorta for collagen fibres in (a) in-plane and (b) out-of-plane directions.

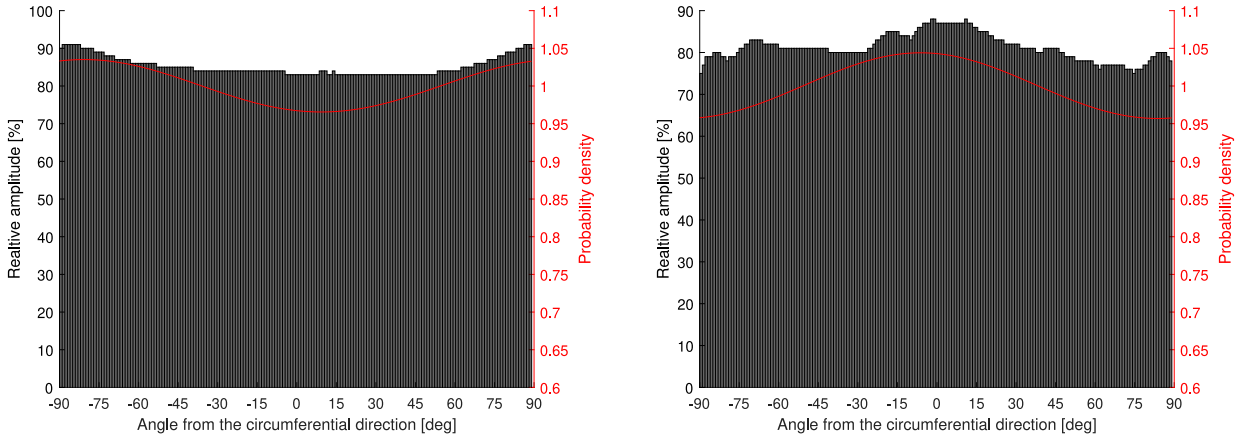

(a) *(b)*

Figure 32: Probability density function of porcine (1) left pulmonary artery for collagen fibres in (a) in-plane and (b) out-of-plane directions.

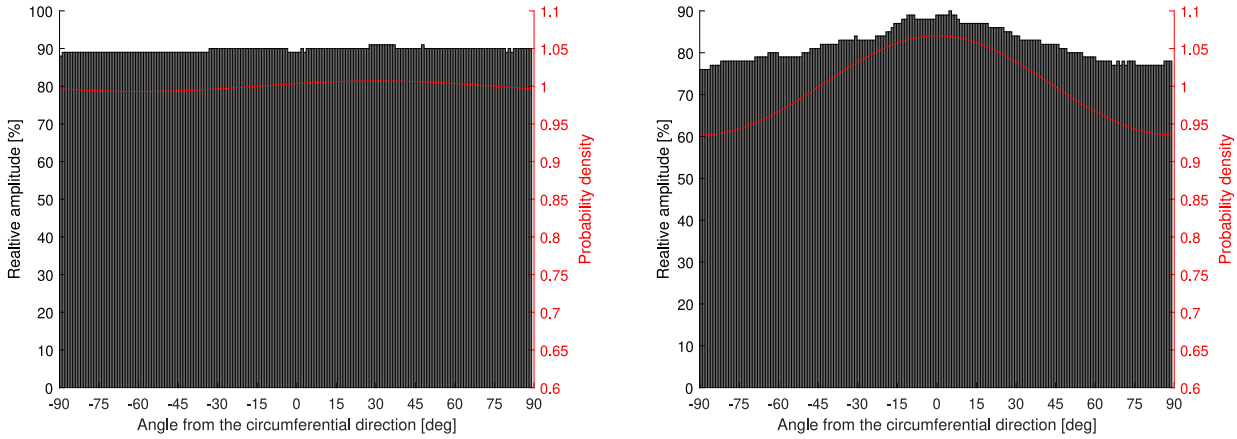

(a) *(b)*

Figure 33: Probability density function of porcine (1) main pulmonary artery for collagen fibres in (a) in-plane and (b) out-of-plane directions.

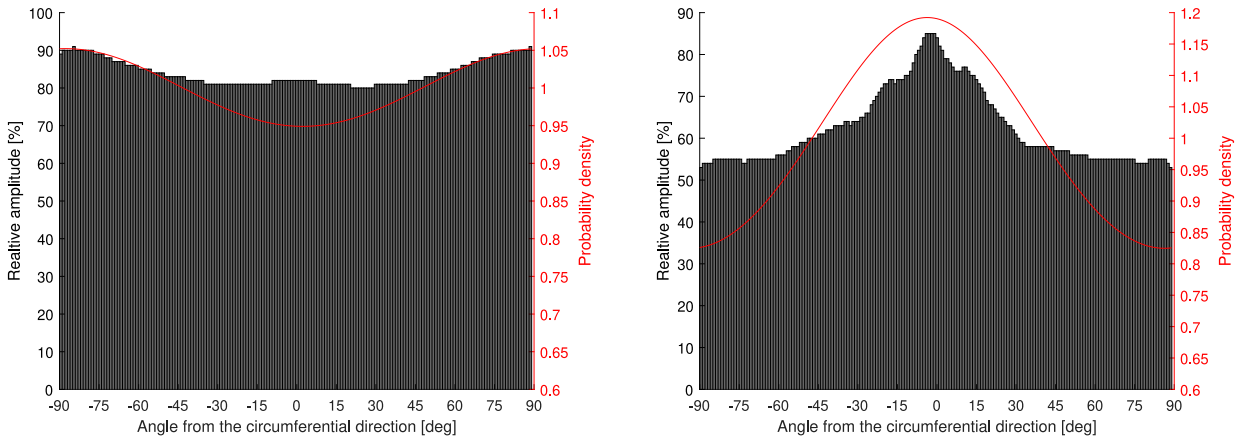

(a) *(b)*

Figure 34: Probability density function of porcine (1) right pulmonary artery for collagen fibres in (a) in-plane and (b) out-of-plane directions.

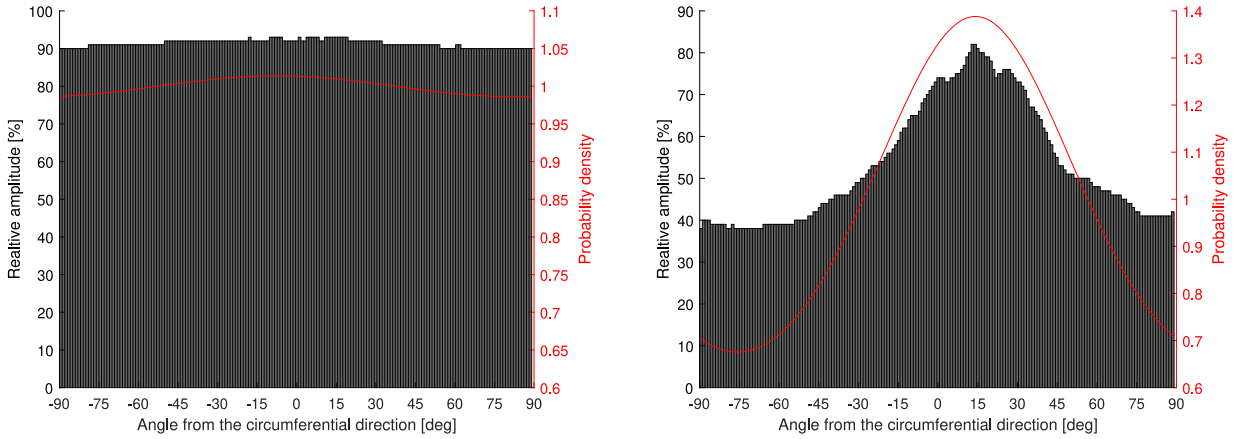

(a) (b)

Figure 35: Probability density function of porcine (2) left pulmonary artery for collagen fibres in (a) in-plane and (b) out-of-plane directions.

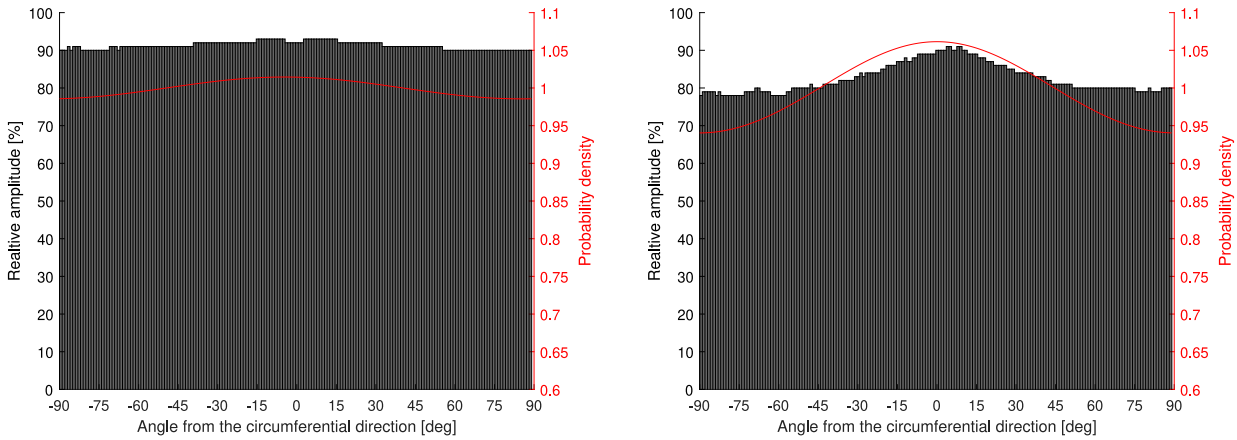

(a) (b)

Figure 36: Probability density function of porcine (2) main pulmonary artery for collagen fibres in (a) in-plane and (b) out-of-plane directions.

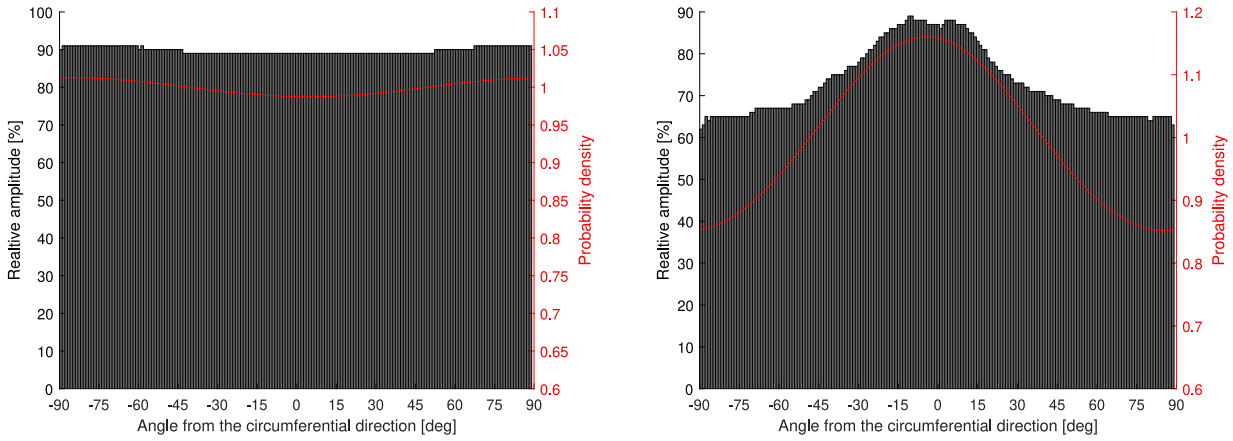

(a) *(b)*

Figure 37: Probability density function of porcine (2) right pulmonary artery for collagen fibres in (a) in-plane and (b) out-of-plane directions.

Summary

The SHG imaging results show that the out-of-plane direction usually displays a narrower distribution, consistent with prior research. However, there are some cases where a slight shift occurs, likely due to imperfect sample arrangement during imaging. Furthermore, the in-plane distribution often appears to be quite isotropic, indicating that additional post-processing may be required to utilize this data for the subsequent deliverable (*Deliverable 9.1 - Constitutive vessel model (TUG, M18)*). It is crucial to note that the distribution heavily depends on the selected region, and areas with lower light intensity (such as artefacts) can result in a more isotropic plot. Therefore, it is imperative to validate the accuracy of the distributions.

Parameter identification

The parameter identification with the related uncertainty quantification is performed in two steps. Firstly, the constitutive parameters are identified by using representative experimental data from the literature from the ascending aorta and the pulmonary artery. To decrease the uncertainties related to experimental data coming from different laboratories, we aim to use as less experimental studies as possible. We used representative experimental data from the literature as the full set of experimental data from our laboratory was initially not available. Secondly, after obtaining the full set of experimental results from our laboratory, the constitutive parameters are determined. Experimental results from our laboratory can then also compared with the available experimental data from literature.

Literature

In the following, experimental results from equibiaxial extension tests obtained from literature are presented. In particular, we reprinted the results obtained in the study of Azadani et al. [1] and Matthews et al. [2]. Azadani et al. [1] performed equibiaxial extension tests on healthy human tissue, especially on the ascending aorta and the pulmonary artery. Similarly, in the study of Matthews et al. [2], equibiaxial extension test results were conducted on fresh porcine tissue, again on the ascending aorta and the pulmonary artery. For the purpose of this delivery, it is advantageous to use data from only two studies. Unfortunately, the literature does not provide appropriate data from sheep tissue.
We have selected representative results of the two studies and reproduced the stress versus stretch curves in *Figures* 38 -39. Note that these studies do not share the original experimental data, so that the stress versus stretch curves were reproduced from the published document.

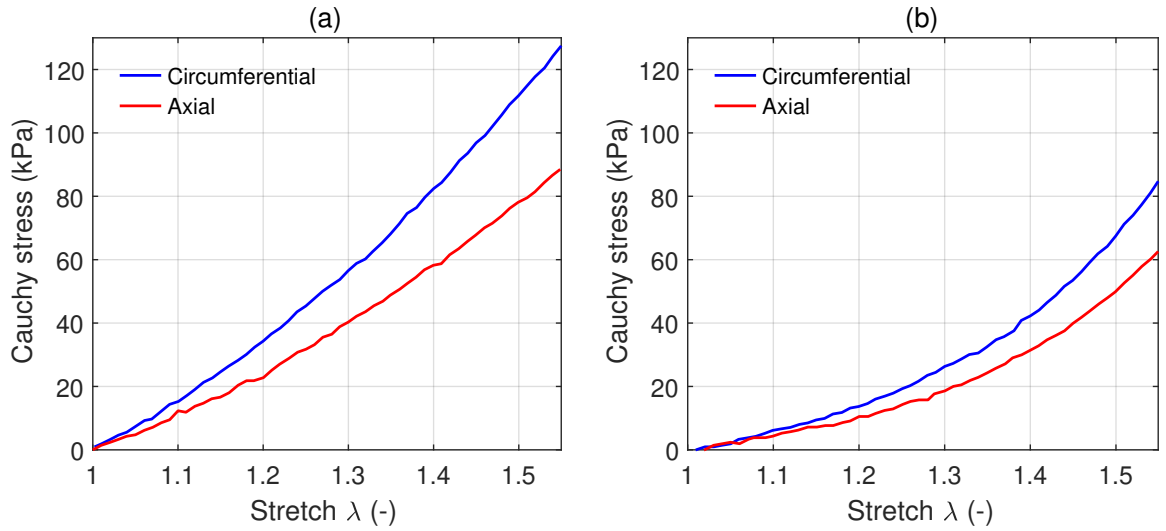

Figure 38: Cauchy stress versus stretch data of a representative (a) porcine ascending aorta and (b) porcine pulmonary artery in circumferential and axial directions. The experimental equibiaxial data is obtained from the study of Matthews et al. [2].

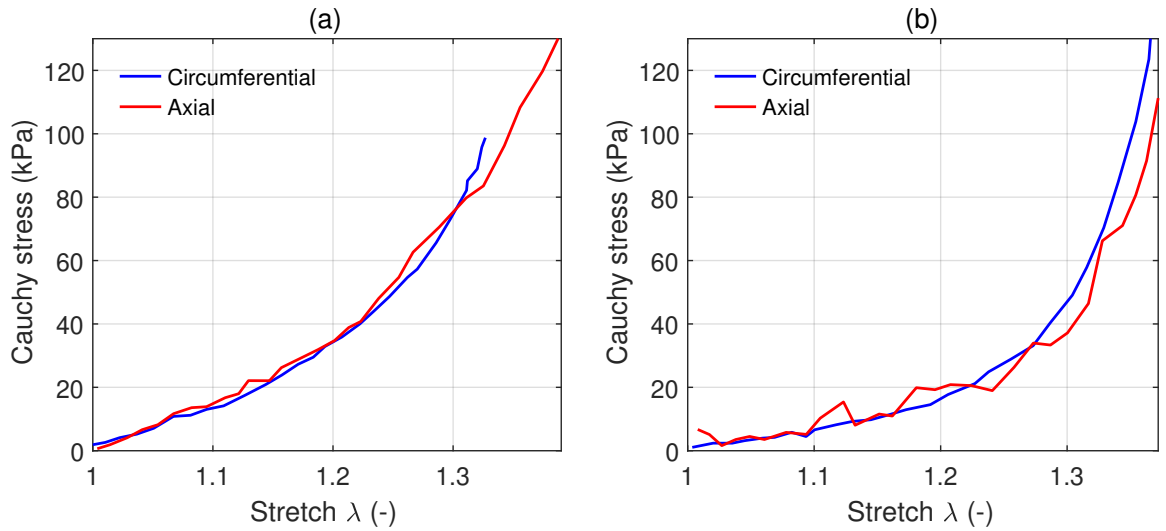

Figure 39: Cauchy stress versus stretch data of a representative (a) human ascending aorta and (b) human pulmonary artery in circumferential and axial directions. The experimental equibiaxial data is obtained from the study of Azadani et al. [1].

Non-linear least squares method

The constitutive parameters were determined by minimising an objective function via nonlinear least-square analysis. The objective function is defined as the sum of the squared differences between the analytically predicted Cauchy stress and the experimental measured values over the number of experimental data points. The required experimental data was obtained from the literature. We implemented the proposed strain–energy functions (see *Deliverable 8.3 - Constitutive vessel model (TUG, M20)*) in MATLAB to obtain the analytical solution of the Cauchy stress for the equibiaxial extension test. Then, the built-in function *lsqnonlin* was used to solve the described minimisation problem.

Results

In the following, the results of the parameter identification with the non-linear least squares methods are presented, see *Tables* 1-2, and *Figures* 40-43.
The results clearly show that the neo-Hookean model can only represent the experimental data well for the chosen stretch values. Due to the exponential material behaviour, it is not possible to fit the experimental data with a neo-Hookean material model that shows a constant gradient. Therefore the model can only be fitted to certain stretch ranges for which it then represents a correct strain-stress relationship. In contrast, the Fung-Demiray model is able to represent the exponential material behaviour well. However, it is unable to account for anisotropy. That is, it is unable to capture the different behaviour in the circumferential and axial directions.

	Stretch	Parameter		
	λ	μ	b	R^2
	(–)	(kPa)	(–)	(–)
Ascending Aorta				
Neo-Hookean model	1.3	30.04	-	0.862
	1.5	37.12	-	0.849
Fung-Demiray model	1.5	27.32	0.27	0.903
Pulmonary Artery				
Neo-Hookean model	1.3	12.87	-	0.857
	1.5	19.72	-	0.791
Fung-Demiray model	1.5	9.98	0.61	0.944

Table 1: Parameter identification of the neo-Hookean (λ=1.3 and λ=1.5) and the Fung-Demiray (λ=1.5) model for porcine ascending aorta and pulmonary artery.

	Stretch	Parameter		
	λ	μ	b	R^2
	(–)	(kPa)	(–)	(–)
Ascending Aorta				
Neo-Hookean model	1.3	39.94	-	0.889
	1.5	51.67	-	0.816
Fung-Demiray model	1.5	24.34	1.11	0.992
Pulmonary Artery				
Neo-Hookean model	1.3	22.00	-	0.800
	1.5	39.07	-	0.599
Fung-Demiray model	1.5	6.39	2.33	0.963

Table 2: Parameter identification of the neo-Hookean (λ=1.3 and λ=1.5) and the Fung-Demiray (λ=1.5) model for human ascending aorta and pulmonary artery.

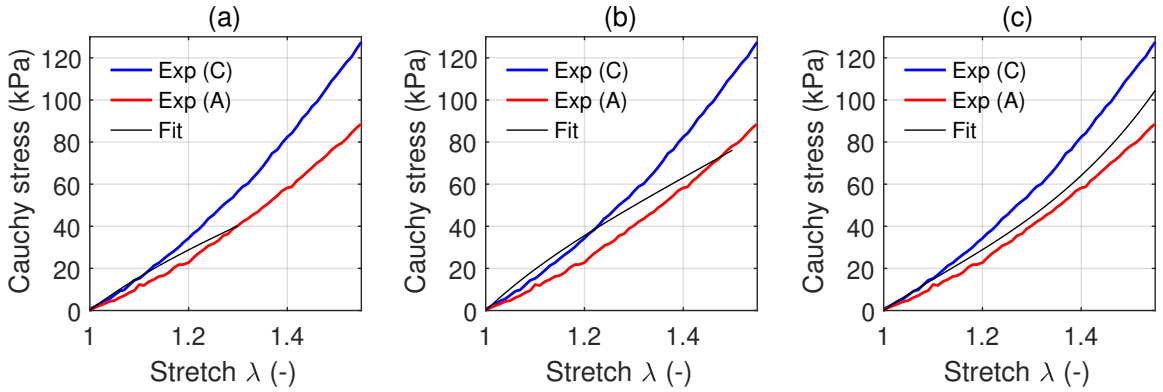

Figure 40: Parameter identification of the neo-Hookean model, for a maximum stretch of λ=1.3 (a) and λ=1.5 (b) and of the Fung-Demiray model for λ=1.5 (c), from porcine ascending aorta. The plots show the comparison between experiments [2] (equibiaxial extension test) and results from parameter identification obtained with MATLAB (C: Circumferential; A: Axial).

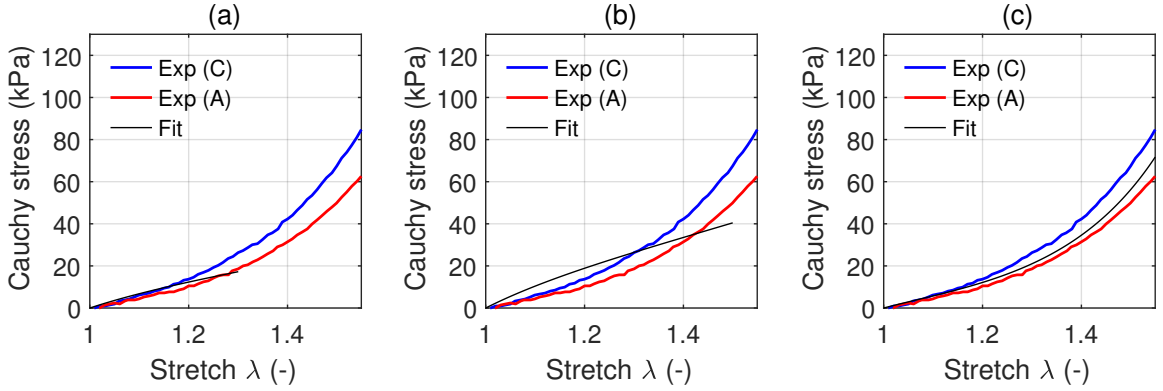

Figure 41: Parameter identification of the neo-Hookean model, for a maximum stretch of λ=1.3 (a) and λ=1.5 (b) and of the Fung-Demiray model for λ=1.5 (c), from porcine pulmonary artery. The plots show the comparison between experiments [2] (equibiaxial extension test) and results from parameter identification obtained with MATLAB (C: Circumferential; A: Axial).

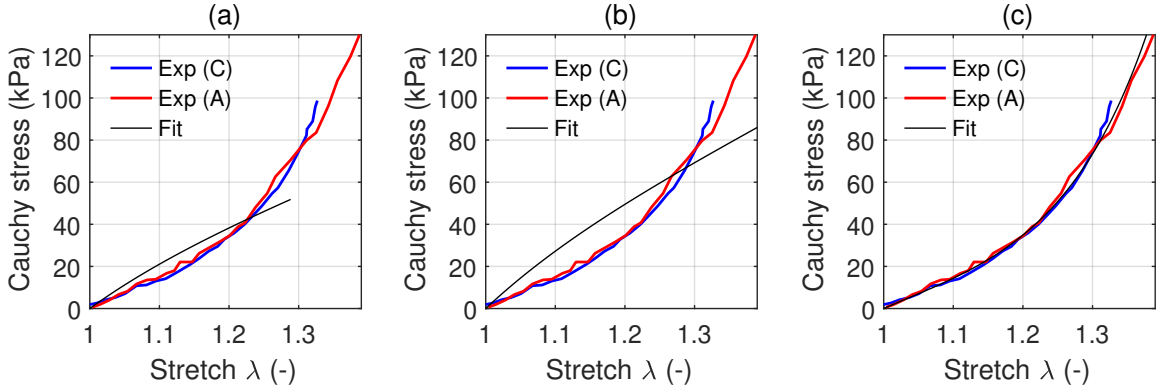

Figure 42: Parameter identification of the neo-Hookean model, for a maximum stretch of λ=1.3 (a) and λ=1.5 (b) and of the Fung-Demiray model for λ=1.5 (c), from human ascending aorta. The plots show the comparison between experiments [2] (equibiaxial extension test) and results from parameter identification obtained with MATLAB (C: Circumferential; A: Axial).

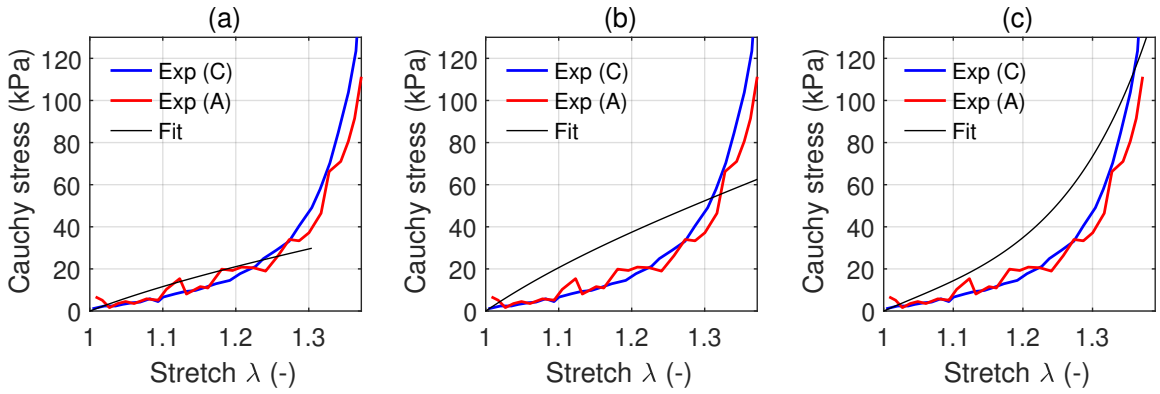

Figure 43: Parameter identification of the neo-Hookean model, for a maximum stretch of λ=1.3 (a) and λ=1.5 (b) and of the Fung-Demiray model for λ=1.5 (c), from human pulmonary artery. The plots show the comparison between experiments [2] (equibiaxial extension test) and results from parameter identification obtained with MATLAB (C: Circumferential; A: Axial).

Laboratory (Institute of Biomechanics, TUG)

In this section we present the results of parameter identification based on the experimental results from our laboratory on porcine, sheep and human samples. Missing information in the tables indicates that the specific tissue sample failed prematurely or data was not suitable for post-processing.

Non-linear least squares method

Similar to the previous section, the constitutive parameters were determined through non-linear least-squares analysis to minimise an objective function. The objective function is defined as the sum of squared differences between the analytically predicted Cauchy stress and the measured experimental values, divided by the number of experimental data points. The experimental data were described in *Section* Test results. To obtain the analytical solution of the Cauchy stress for the equibiaxial extension test, we utilised the proposed strain-energy functions (see *Deliverable 8.3 - Constitutive vessel model (TUG, M20)*) in MATLAB. We then utilised the built-in function *lsqnonlin* to solve the minimisation problem as described.

Results

In the following, the results of the parameter identification with the non-linear least squares methods are presented. The material parameters determined for the neo-Hookean and Fung-Demiray models are reported in *Tables* 3-5. The stress versus stretch curves from the experiments and those predicted by the model fitting are shown in and *Figures* 44-55 in the Appendix. Equibiaxial extension results (strain ratio 1:1) were fitted until failure stretch with the Fung-Demiray model. With the neo-Hookean model we have fitted the experimental curves until a threshold stretch $\lambda = 1.3$ or until failure if this occurred before the threshold.
As already observed for the experimental data from the literature, the results show that the neo-Hookean model can represent the experimental data only at low stretches and limited to the cases in which the stiffening is limited, as for instance in sheep or porcine ascending aorta. It is unable to provide a satisfactory fit for the human tissue, where such stiffening effect is very pronounced. In contrast, the Fung-Demiray model is able to represent the exponential material behaviour well. However, it is unable to account for anisotropy, that is, it cannot capture the different behaviour in the circumferential and axial direction. In general, care should be taken when evaluating the fitting performance based on the R^2 value, since this is a poor indicator for nonlinear regression analysis.

Ascending Aorta											
Sample	1	2	3	4	5	6	7	8	9	10	11
NH – μ (kPa)	37.35	37.07	44.03	60.49	70.67	76.32	44.30	43.24	65.81	71.45	42.08
NH – R^2 (–)	0.921	0.978	0.966	0.948	0.974	0.950	0.971	0.982	0.968	0.981	0.893
FD – μ (kPa)	32.24	28.54	33.54		55.50	61.91	35.35	31.45		61.59	33.55
FD – b (–)	0.35	0.48	0.56		0.55	0.91	0.50	0.48		0.63	0.50
FD – R^2 (–)	0.949	0.990	0.997		0.996	0.971	0.993	0.994		0.989	0.907
Main Pulmonary Artery											
Sample	1	2	3	4	5	6	7	8	9	10	11
NH – μ (kPa)	18.58	6.98	10.70	8.19	9.21		8.90	9.05	5.99	9.03	7.25
NH – R^2 (–)	0.900	0.880	0.969	0.884	0.886		0.979	0.892	0.954	0.925	0.964
FD – μ (kPa)	10.48	3.12	4.88	3.16	3.96		4.62	4.38	2.64	6.60	5.49
FD – b (–)	1.25	0.89	0.75	0.90	0.85		0.62	0.73	0.63	0.53	0.46
FD – R^2 (–)	0.997	0.939	0.959	0.944	0.970		0.976	0.860	0.965	0.977	0.974
Left Pulmonary Artery											
Sample	1	2	3	4	5	6	7	8	9	10	11
NH – μ (kPa)	21.80	16.75	16.81	13.70	20.13		12.79	23.74	10.34	23.07	14.74
NH – R^2 (–)	0.813	0.837	0.899	0.855	0.860		0.888	0.878	0.947	0.842	0.966
FD – μ (kPa)	11.40	10.44	10.77	7.04	10.51		6.86	11.53	6.76	13.21	9.65
FD – b (–)	1.41	0.99	0.97	1.40	1.34		1.27	1.47	0.62	1.23	0.71
FD – R^2 (–)	0.946	0.891	0.942	0.996	0.997		0.919	0.988	0.966	0.943	0.977
Right Pulmonary Artery											
Sample	1	2	3	4	5	6	7	8	9	10	11
NH – μ (kPa)	24.73	14.31	22.03	12.07	20.49	9.64	19.41		20.61	10.11	25.29
NH – R^2 (–)	0.775	0.937	0.795	0.855	0.864	0.840	0.924		0.723	0.917	0.786
FD – μ (kPa)	13.35	9.19	9.68	6.51	12.33	6.34	10.44		8.52	7.49	11.94
FD – b (–)	1.37	0.81	1.75	1.35	1.12	0.82	1.14		1.92	0.65	1.64
FD – R^2 (–)	0.895	0.966	0.998	0.992	0.967	0.858	0.995		0.905	0.977	0.935

Table 3: Parameter identification of the neo-Hookean (NH) ($\lambda = 1.3$) and the Fung-Demiray (FD) model for porcine ascending aorta and pulmonary artery.

Ascending Aorta									
Sample	1	2	3	4	5	6	7	8	9
NH – μ (kPa)	10.65	20.88	54.57	17.81	35.31	26.83	48.24	44.01	27.16
NH – R^2 (–)	0.820	0.804	0.976	0.905	0.974	0.652	0.931	0.885	0.937
FD – μ (kPa)	10.52	15.41	53.77	12.83	32.76	20.16	42.37	33.18	24.07
FD – b (–)	0.48	0.67	0.07	0.72	0.18	0.62	0.30	0.56	0.32
FD – R^2 (–)	0.983	0.924	0.976	0.972	0.976	0.682	0.939	0.904	0.974
Main Pulmonary Artery									
Sample	1	2	3	4	5	6	7	8	9
NH – μ (kPa)	9.67	8.92	8.84	13.00	3.99	2.93			9.95
NH – R^2 (–)	0.947	0.914	0.959	0.907	0.843	0.896			0.944
FD – μ (kPa)	3.36	6.72	3.96	7.81	3.43	2.80			7.50
FD – b (–)	1.45	0.64	1.41	1.13	0.56	0.45			0.53
FD – R^2 (–)	0.967	0.947	0.951	0.999	0.986	0.987			0.966
Left Pulmonary Artery									
Sample	1	2	3	4	5	6	7	8	9
NH – μ (kPa)	9.09	6.84	7.08	5.12	3.94				
NH – R^2 (–)	0.940	0.929	0.909	0.930	0.925				
FD – μ (kPa)	6.39	0.55	4.85	3.72	2.19				
FD – b (–)	0.63	1.92	0.84	0.51	0.80				
FD – R^2 (–)	0.993	0.931	0.997	0.966	0.981				
Right Pulmonary Artery									
Sample	1	2	3	4	5	6	7	8	9
NH – μ (kPa)		4.72	5.47	6.62	4.63				
NH – R^2 (–)		0.874	0.961	0.732	0.896				
FD – μ (kPa)		2.78	3.34	4.23	3.46				
FD – b (–)		0.88	0.59	1.85	0.66				
FD – R^2 (–)		0.967	0.989	0.813	0.987				

Table 4: Parameter identification of the neo-Hookean (NH) ($\lambda = 1.3$) and the Fung-Demiray (FD) model for sheep ascending aorta and pulmonary artery.

Ascending Aorta					
Sample	1	2	3	4	5
NH – μ (kPa)		19.94	41.48		
NH – R^2 (–)		0.840	0.629		
FD – μ (kPa)		4.10	3.49		
FD – b (–)		2.96	4.27		
FD – R^2 (–)		0.986	0.948		
Main Pulmonary Artery					
Sample	1	2	3	4	5
NH – μ (kPa)	45.22	10.24	10.62	13.05	24.77
NH – R^2 (–)	0.408	0.879	0.866	0.786	0.500
FD – μ (kPa)	0.67	1.84	1.26	5.39	0.42
FD – b (–)	8.37	2.53	3.39	1.83	9.07
FD – R^2 (–)	0.969	0.970	0.915	0.880	0.890
Left Pulmonary Artery					
Sample	1	2	3	4	5
NH – μ (kPa)	58.97		25.01	10.87	30.41
NH – R^2 (–)	0.517		0.565	0.839	0.481
FD – μ (kPa)	3.22		0.41	1.34	1.09
FD – b (–)	10.38		10.85	3.23	11.63
FD – R^2 (–)	0.987		0.930	0.954	0.940
Right Pulmonary Artery					
Sample	1	2	3	4	5
NH – μ (kPa)	52.17	27.60	35.37	11.84	18.17
NH – R^2 (–)	0.444	0.556	0.561	0.836	0.728
FD – μ (kPa)	0.83	0.91	2.47	5.03	4.97
FD – b (–)	23.54	5.65	4.84	3.49	17.18
FD – R^2 (–)	0.970	0.887	0.985	0.998	0.973

Table 5: Parameter identification of the neo-Hookean (NH) ($\lambda = 1.3$) and the Fung-Demiray (FD) model for human ascending aorta and pulmonary artery.

Discussion

The biaxial extension tests were successfully carried out with the experimental set-up available in the laboratory of the Institute of Biomechanics at TUG. We were able to follow the defined experimental protocol and obtain repeatable results for the tests performed. The results of the biaxial extension tests show the characteristic exponential stiffening of the tissue at higher stretches. Interestingly, as outlined above, the ascending aorta and pulmonary artery showed different material behaviour. In addition, porcine and human tissue tends to be stiffer than sheep tissue. Even if the experiments are repeatable, the variation between the different samples is fairly high. The observed variability in the experiments was expected, as human and animal tissue usually show a high variability, and was not artificially minimised by altering the processing approach, as this would not quantify the uncertainty related to the characterisation method. Furthermore, we could not identify experimental errors that could have led to this variability.
The results of the parameter identification showed that the Fung-Demiray model shows a significantly improved fit to the experimental data from both the literature and our laboratory. In comparison to the neo-Hookean model, it is able to follow the experimental data for all stretches fairly well. The neo-Hookean model is only able to reproduce the experimental data for small strain regions to which it is fitted, and only for tissues with limited stiffening.

References

[1] A.N. Azadani, S. Chitsaz, P.B. Matthews, N. Jaussaud, J. Leung, A. Wisneski, L. Ge, and E.E. Tseng. Biomechanical comparison of human pulmonary and aortic roots. *Eur J Cardiothorac Surg*, 41(5):1111–6, 2012.

[2] P.B. Matthews, A.N. Azadani, C.-S. Jhun, L. Ge, T.S. Guy, J.M. Guccione, and E.E. Tseng. Comparison of porcine pulmonary and aortic root material properties. *Ann Thorac Surg*, 89(6):1981–1988, 2010.

[3] A. Pukaluk, H. Wolinski, C. Viertler, P. Regitnig, G. A. Holzapfel, and G. Sommer. An approach for visualization of the interaction between collagen and elastin in loaded human aortic tissues. In *Proc. Annual Meeting of the Austrian Society for Biomedical Engineering 2021*, pages 21–24. Verlag der Technischen Universität Graz, 2021.

[4] A.J. Schriefl, H. Wolinski, P. Regitnig, S.D. Kohlwein, and Holzapfel G.A. An automated approach for three-dimensional quantification of fibrillar structures in optically cleared soft biological tissues. *J. R. Soc. Interface*, 10:20120760, 2013.

Appendix

Supplementary material - Biaxial extension test

		Mean thickness (mm)	Sample size (mm)
S1	AA	2.84	10x10
	MPA	2.69	10x10
	LPA	1.18	10x10
S2	AA	1.97	10x10
	MPA	3.50	10x10
	LPA	1.34	10x10
	RPA	1.82	11x11
S3	AA	3.96	10x11
	MPA	3.35	10x10
	LPA	1.47	10x10
	RPA	1.60	10x10
S4	AA	2.52	11x11
	MPA	3.07	10x10
	LPA	1.27	10x10
	RPA	1.09	10x10
S5	AA	3.35	11x11
	MPA	2.42	11x11
	LPA	1.55	10x10
	RPA	1.09	10x10
S6	AA	2.63	10x10
	MPA	2.31	9x9
S7	AA	3.62	10x10
S8	AA	3.64	10x10
S9	AA	3.03	11x11
	MPA	3.20	10x10

Table 6: Measured mean thickness and sample size of the sheep tissue samples (AA: Ascending aorta; MPA: Main pulmonary artery; LPA: Left pulmonary artery; RPA: Right pulmonary artery).

		Mean thickness (mm)	Sample size (mm)
P1	AA	2.43	10x10
	MPA	2.48	10x10
	LPA	0.63	10x10
	RPA	0.83	10x10
P2	AA	2.46	10x10
	MPA	2.46	10.5x10.5
	LPA	1.17	10x10
	RPA	0.94	10x10
P3	AA	2.13	10x10
	MPA	1.77	10x10
	LPA	0.79	10x10
	RPA	0.90	10x10
P4	AA	2.13	10x10
	MPA	2.14	10x10
	LPA	0.87	10x10
	RPA	0.79	10x10
P5	AA	2.16	10x10
	MPA	2.04	10x10
	LPA	0.98	10x10
	RPA	0.77	10x10
P6	AA	2.7	10x10
	RPA	1.06	10x10
P7	AA	2.46	10x10
	MPA	2.16	10x10
	LPA	0.87	10x10
	RPA	1.01	10x10
P8	AA	2.87	10x10
	MPA	2.17	10x10
	LPA	0.77	10x10
P9	AA	2.12	10x10
	MPA	2.69	9x9
	LPA	0.81	10x10
	RPA	0.82	10x10
P10	AA	2.6	10x10

	MPA	1.73	10x10
	LPA	0.82	10x10
	RPA	0.67	10x10
P11	AA	2.18	9x9
	MPA	2.28	10x10
	LPA	0.76	10x10
	RPA	0.73	10x10

Table 7: Measured mean thickness and sample size of the porcine tissue samples (AA: Ascending aorta; MPA: Main pulmonary artery; LPA: Left pulmonary artery; RPA: Right pulmonary artery).

		Mean thickness (mm)	Sample size (mm)
H1	MPA	1.39	10x10
	LPA	0.73	9x9
	RPA	0.98	10x10
H2	AA	2.05	10x10
	MPA	1.78	10x10
	RPA	1.16	10x10
H3	AA	1.66	10x10
	MPA	1.21	10x10
	LPA	1.37	10x10
	RPA	1.22	10x10
H4	MPA	1.31	10x10
	LPA	1.21	10x10
	RPA	1.21	10x10
H5	MPA	1.52	10x10
	LPA	1.13	10x10
	RPA	1.15	10x10

Table 8: Measured mean thickness and sample size of the human tissue samples (AA: Ascending aorta; MPA: Main pulmonary artery; LPA: Left pulmonary artery; RPA: Right pulmonary artery).

Supplementary material - Parameter identification (Porcine)

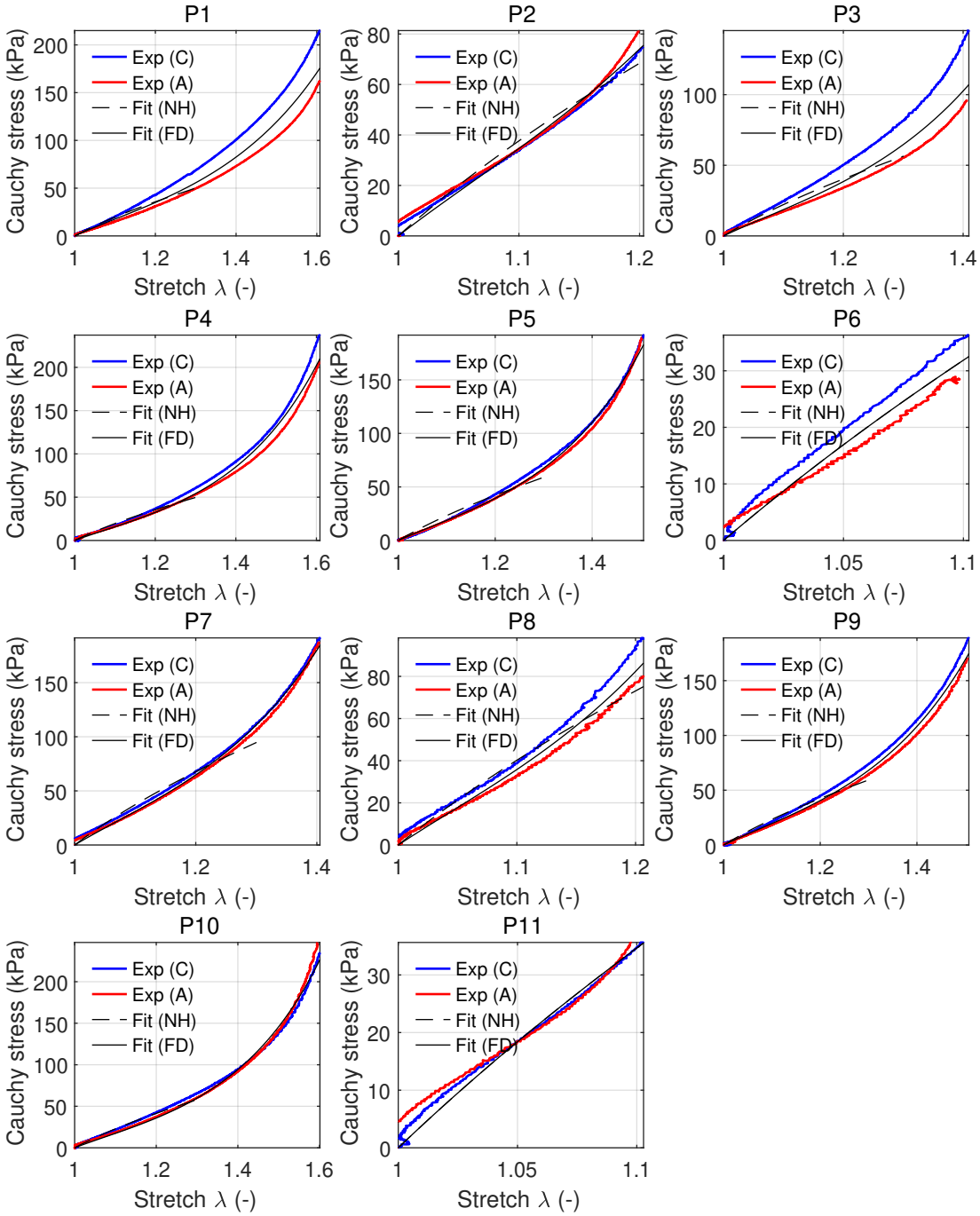

Figure 44: Parameter identification of neo-Hookean (NH) and Fung-Demiray (FD) models for porcine ascending aorta. The plots show the comparison between experiments and results from parameter identification obtained with MATLAB (C: Circumferential; A: Axial).

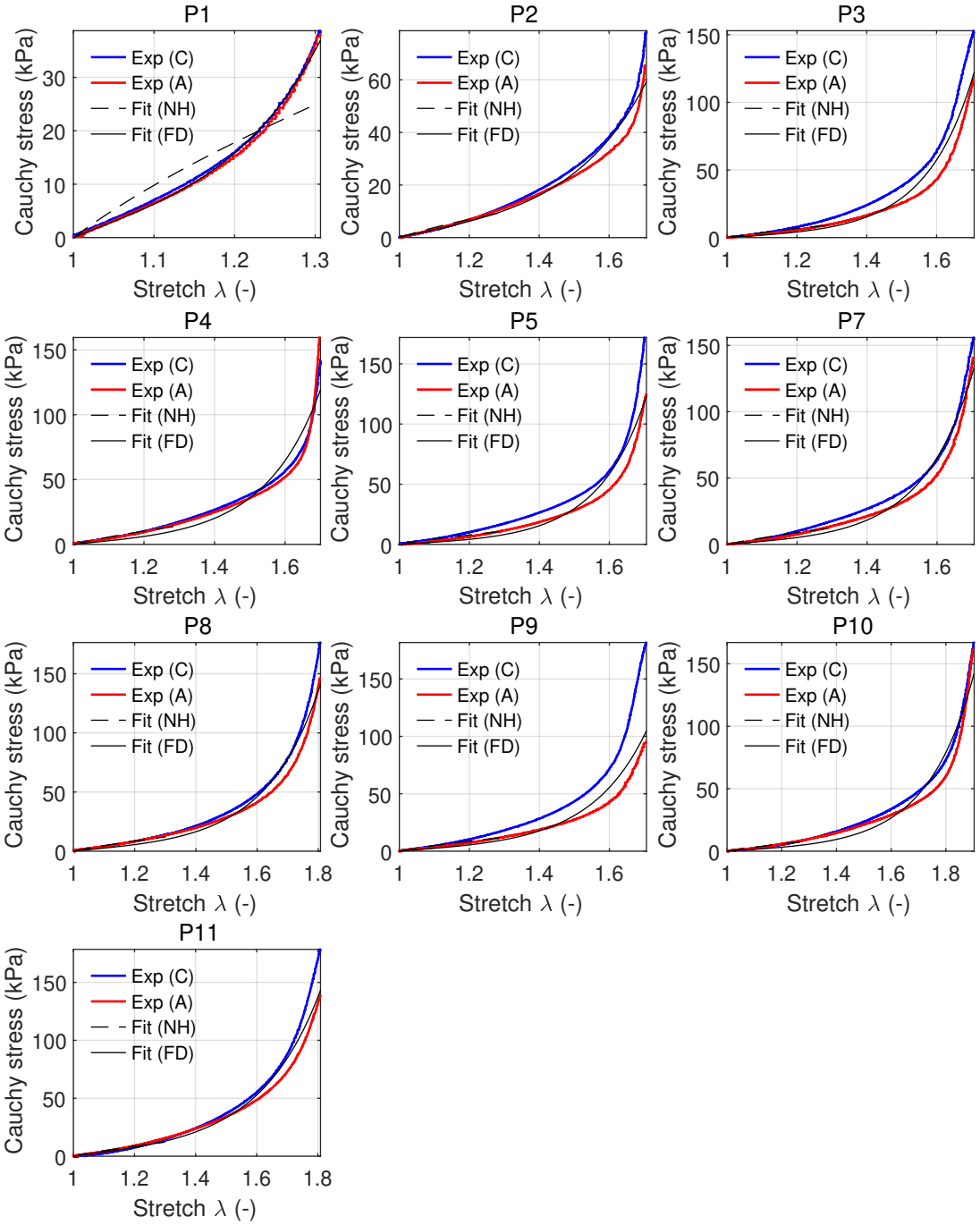

Figure 45: Parameter identification of neo-Hookean (NH) and Fung-Demiray (FD) models for porcine main pulmonary artery. The plots show the comparison between experiments and results from parameter identification obtained with MATLAB (C: Circumferential; A: Axial).

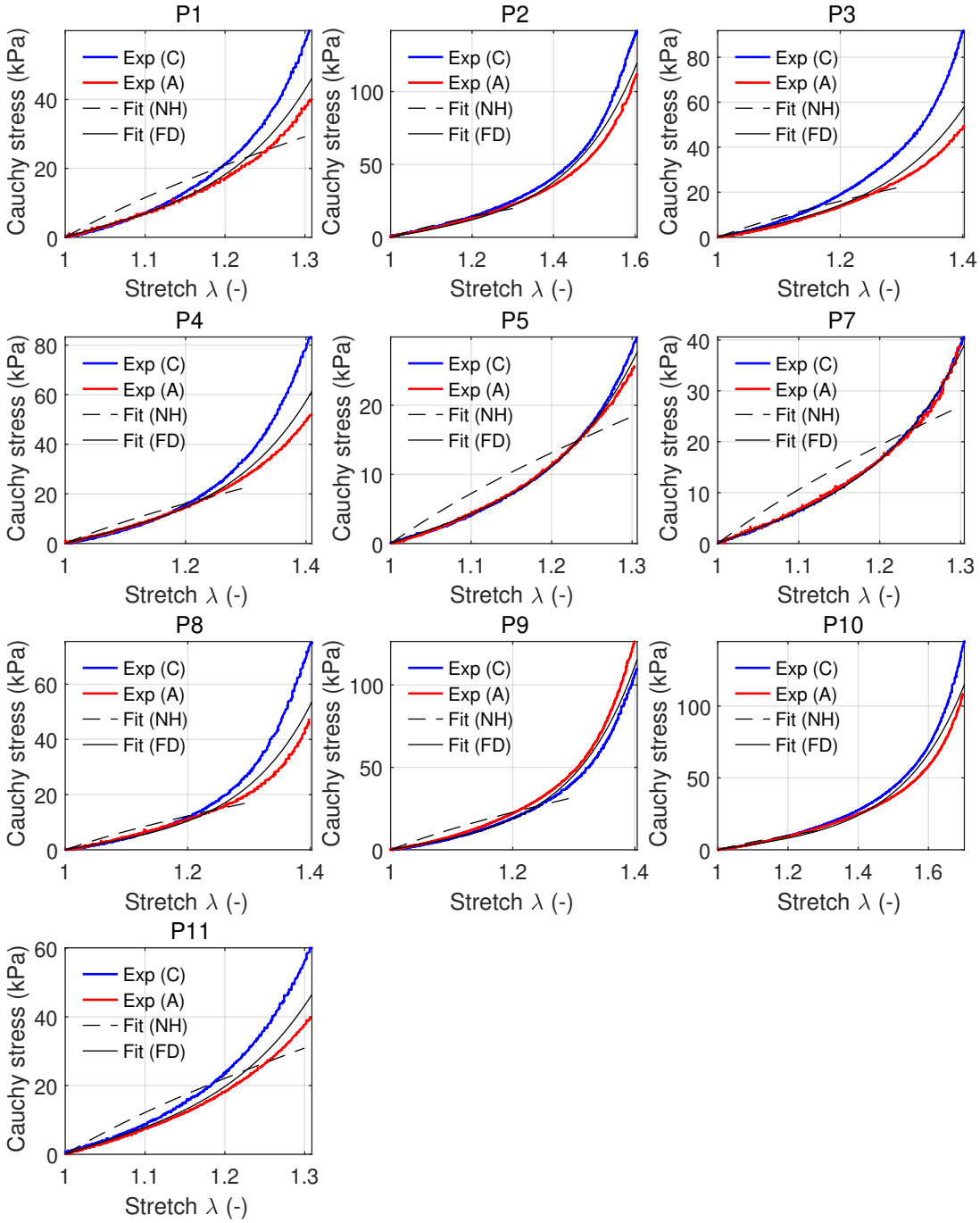

Figure 46: Parameter identification of neo-Hookean (NH) and Fung-Demiray (FD) models for porcine left pulmonary artery. The plots show the comparison between experiments and results from parameter identification obtained with MATLAB (C: Circumferential; A: Axial).

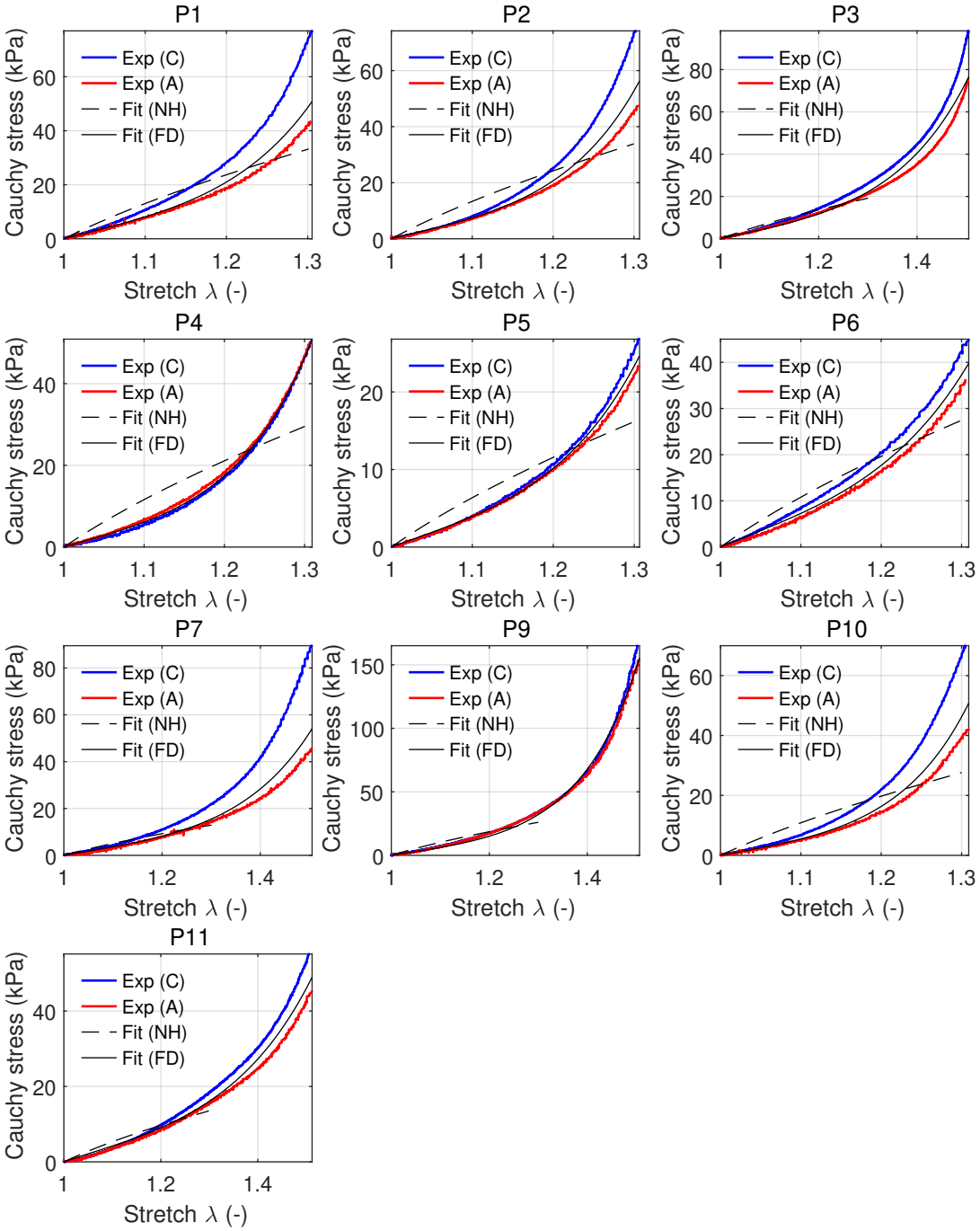

Figure 47: Parameter identification of neo-Hookean (NH) and Fung-Demiray (FD) models for porcine right pulmonary artery. The plots show the comparison between experiments and results from parameter identification obtained with MATLAB (C: Circumferential; A: Axial).

Supplementary material - Parameter identification (Sheep)

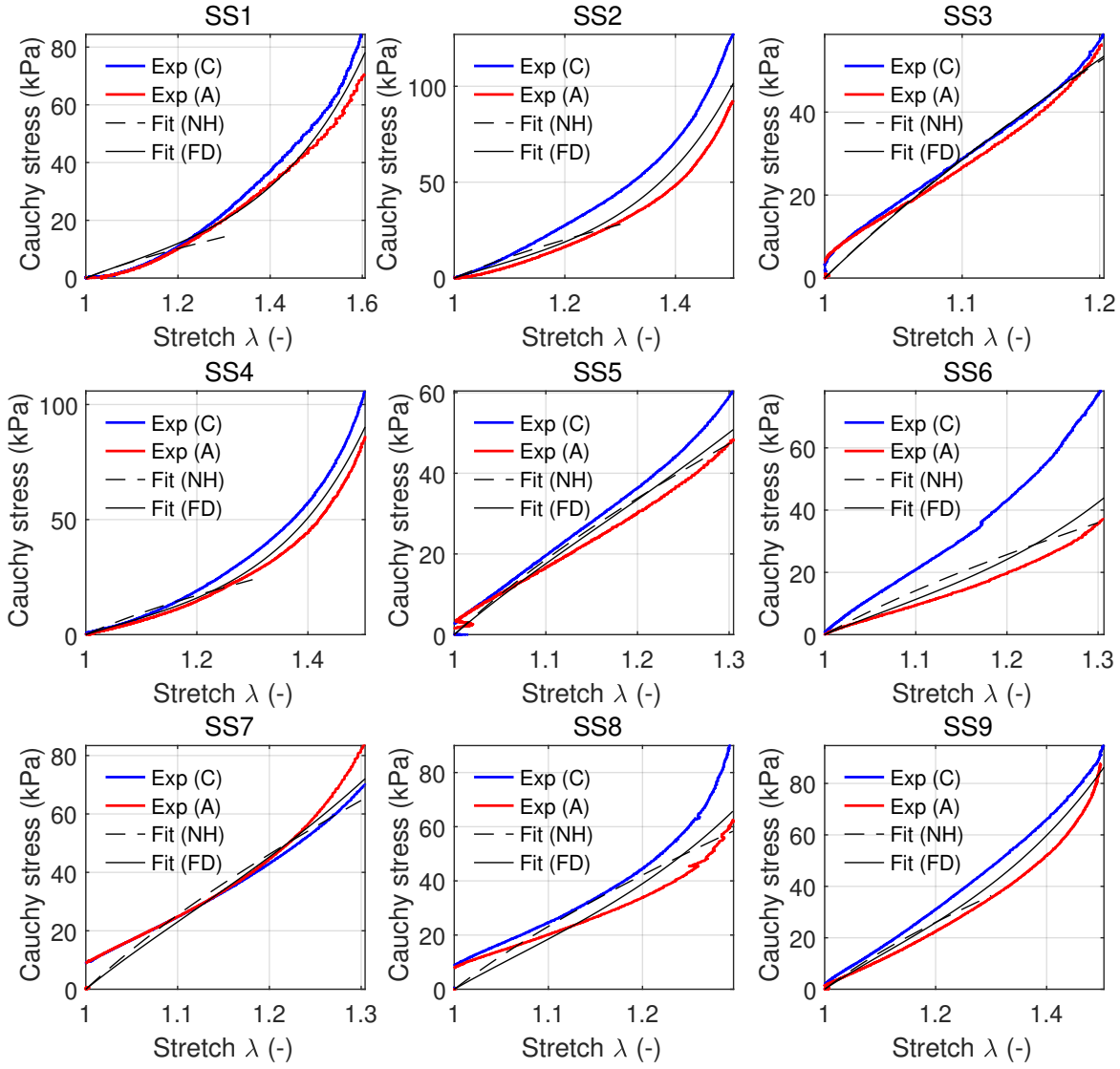

Figure 48: Parameter identification of neo-Hookean (NH) and Fung-Demiray (FD) models for sheep ascending aorta. The plots show the comparison between experiments and results from parameter identification obtained with MATLAB (C: Circumferential; A: Axial).

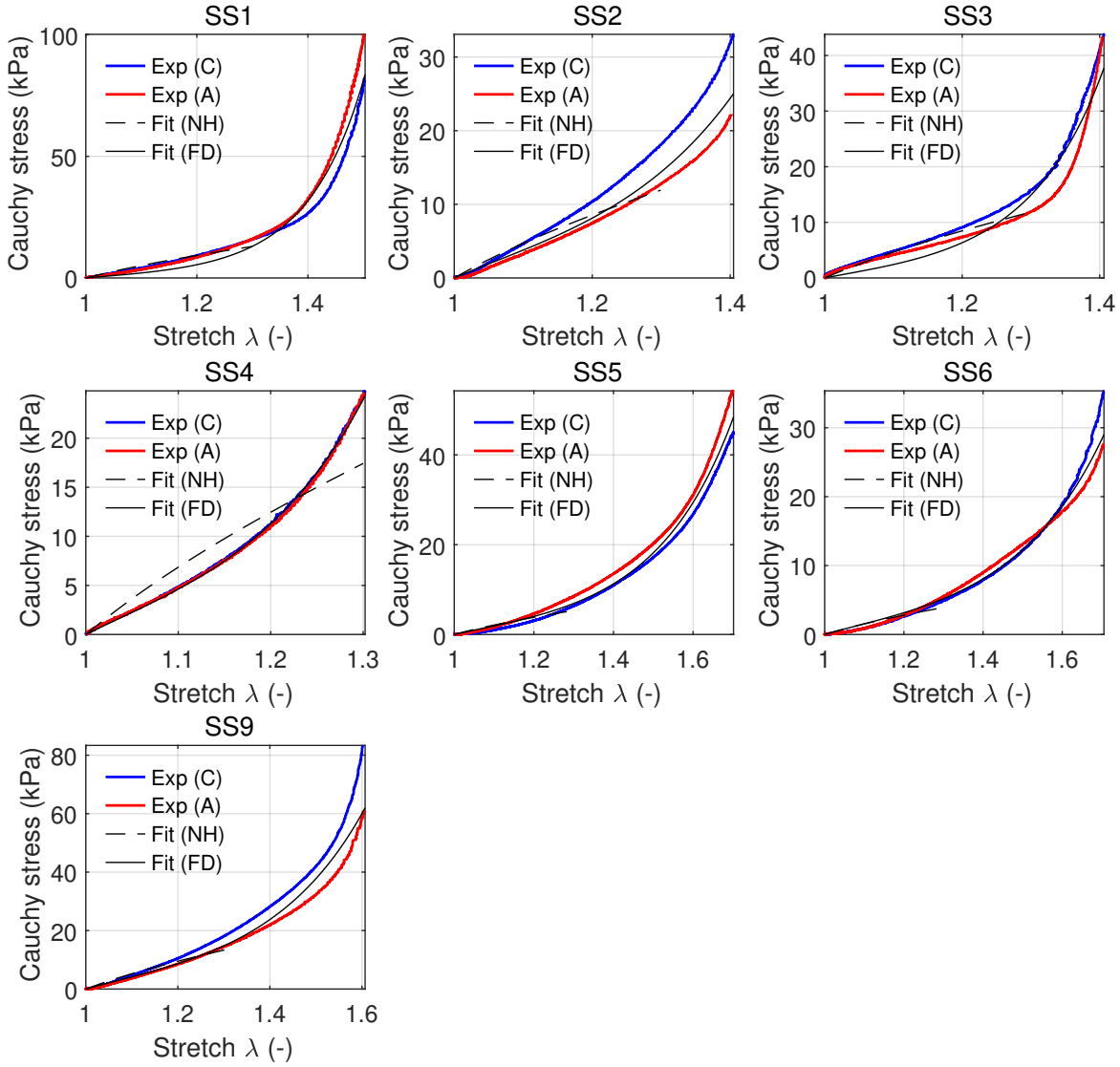

Figure 49: Parameter identification of neo-Hookean (NH) and Fung-Demiray (FD) models for sheep main pulmonary artery. The plots show the comparison between experiments and results from parameter identification obtained with MATLAB (C: Circumferential; A: Axial).

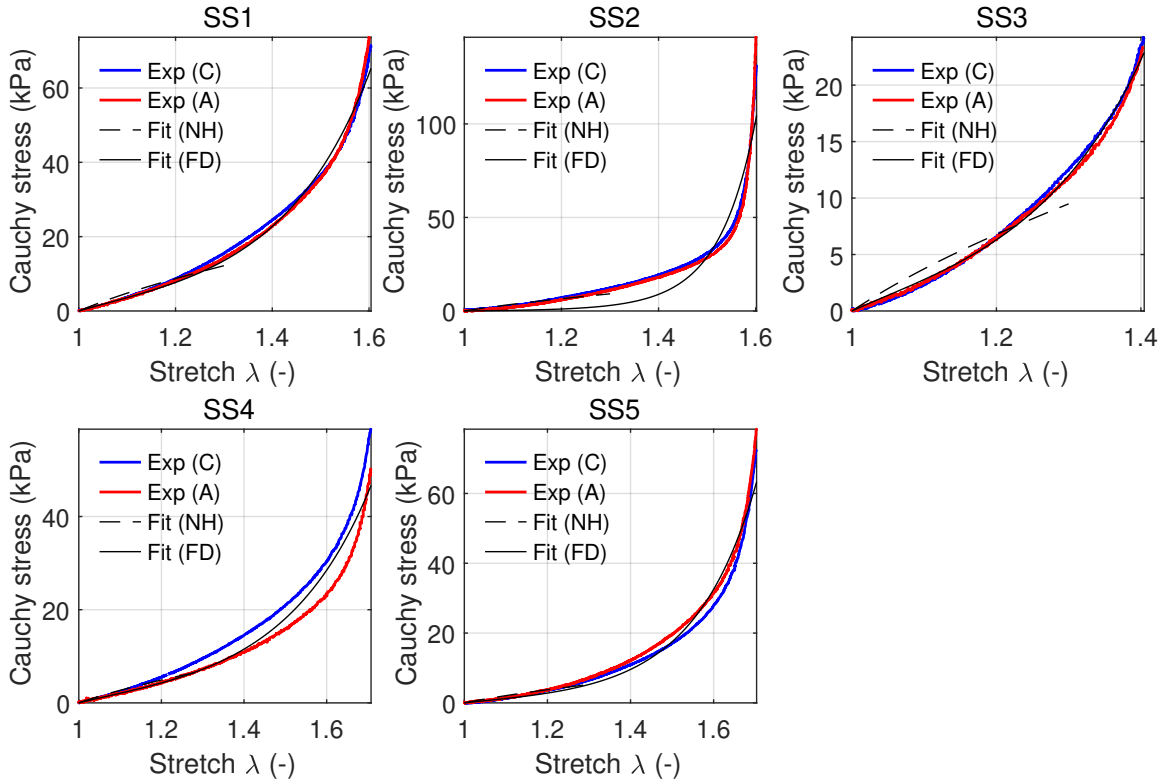

Figure 50: Parameter identification of neo-Hookean (NH) and Fung-Demiray (FD) models for sheep left pulmonary artery. The plots show the comparison between experiments and results from parameter identification obtained with MATLAB (C: Circumferential; A: Axial).

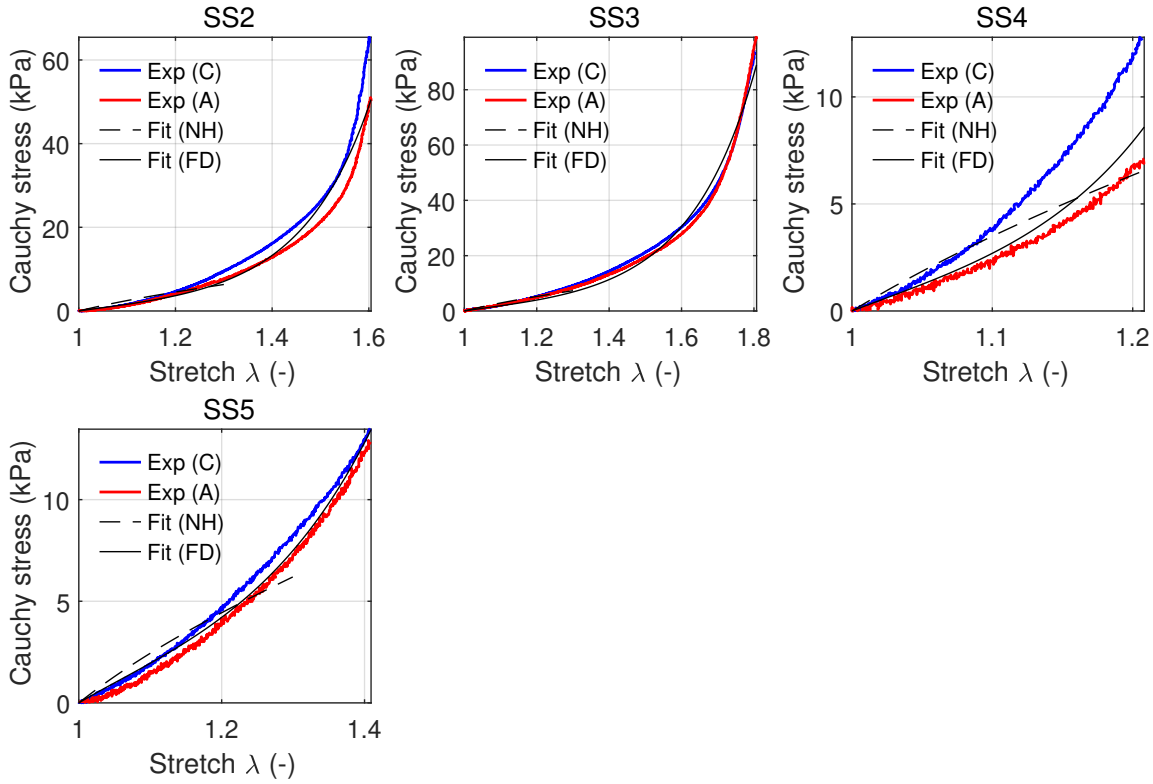

Figure 51: Parameter identification of neo-Hookean (NH) and Fung-Demiray (FD) models for sheep right pulmonary artery. The plots show the comparison between experiments and results from parameter identification obtained with MATLAB (C: Circumferential; A: Axial).

Supplementary material - Parameter identification (Human)

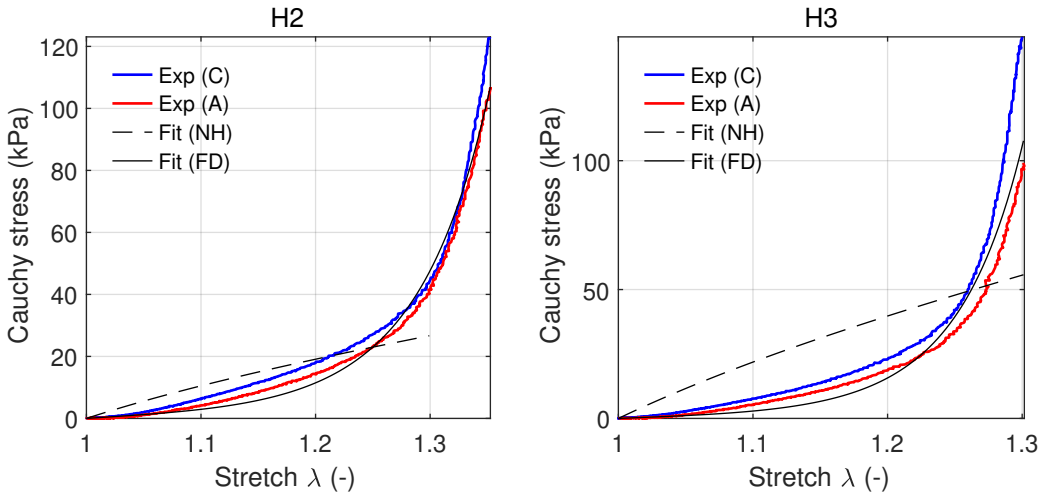

Figure 52: Parameter identification of neo-Hookean (NH) and Fung-Demiray (FD) models for human ascending aorta. The plots show the comparison between experiments and results from parameter identification obtained with MATLAB (C: Circumferential; A: Axial).

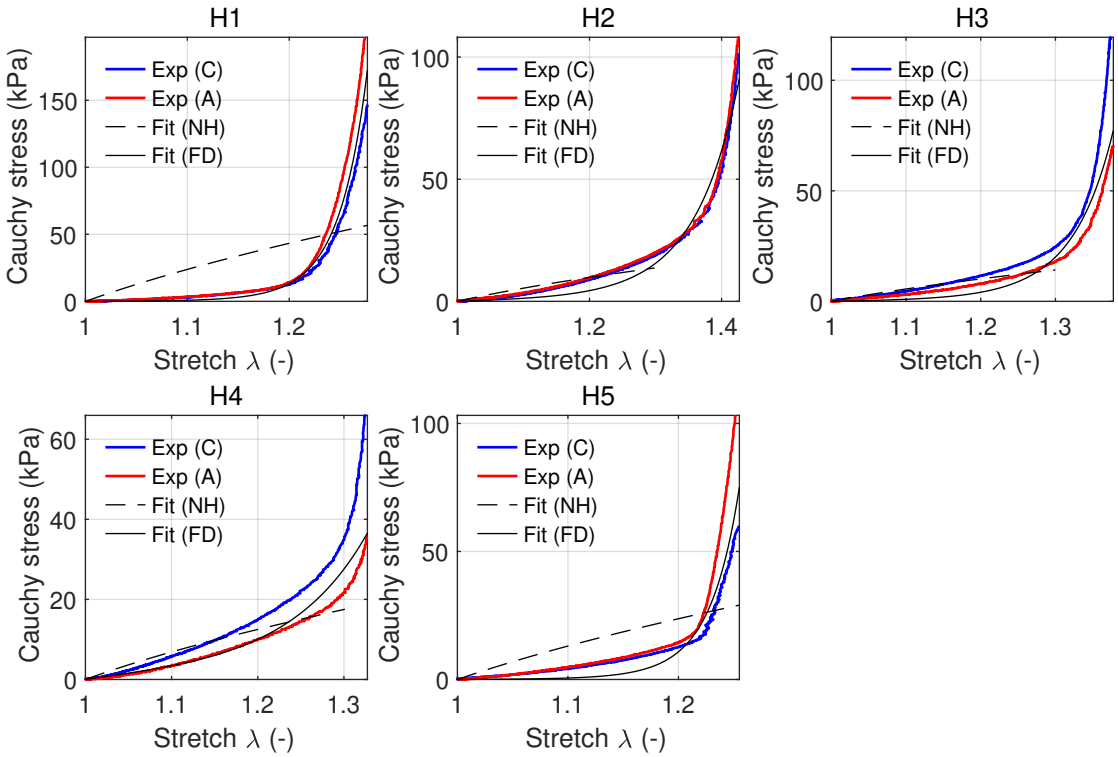

Figure 53: Parameter identification of neo-Hookean (NH) and Fung-Demiray (FD) models for human main pulmonary artery. The plots show the comparison between experiments and results from parameter identification obtained with MATLAB (C: Circumferential; A: Axial).

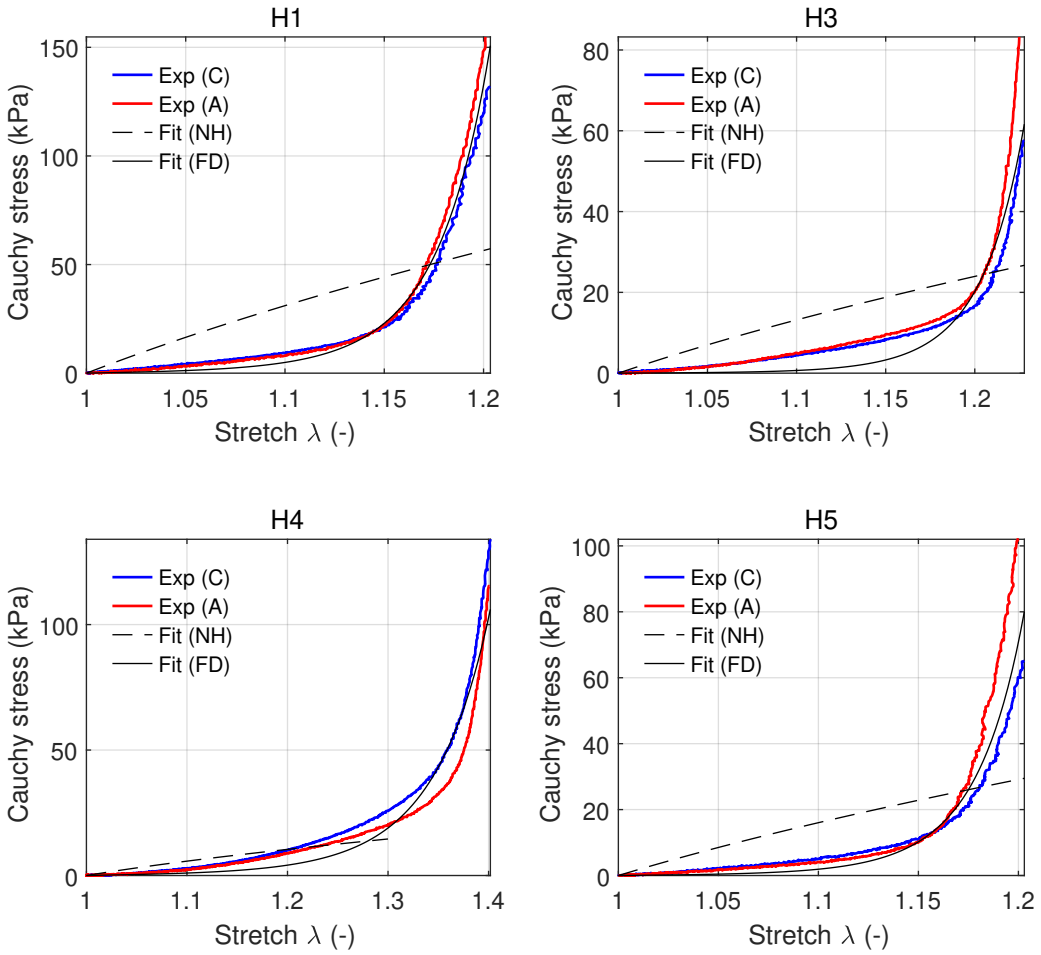

Figure 54: Parameter identification of neo-Hookean (NH) and Fung-Demiray (FD) models for human left pulmonary artery. The plots show the comparison between experiments and results from parameter identification obtained with MATLAB (C: Circumferential; A: Axial).

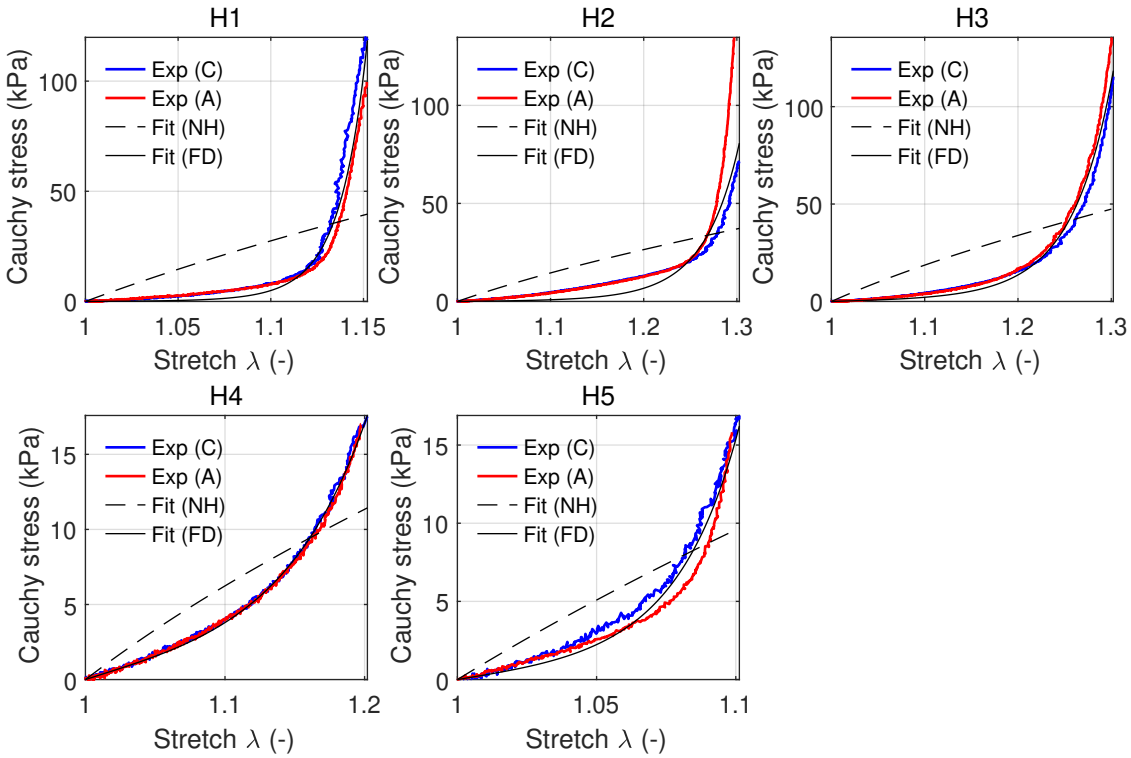

Figure 55: Parameter identification of neo-Hookean (NH) and Fung-Demiray (FD) models for human right pulmonary artery. The plots show the comparison between experiments and results from parameter identification obtained with MATLAB (C: Circumferential; A: Axial).